

Universiteit
Leiden
The Netherlands

Harnessing the immunostimulatory properties of oncolytic reovirus for anticancer immunotherapy

Groeneveldt, P.C.

Citation

Groeneveldt, P. C. (2023, November 23). *Harnessing the immunostimulatory properties of oncolytic reovirus for anticancer immunotherapy*. Retrieved from https://hdl.handle.net/1887/3663612

Version:	Publisher's Version
License:	Licence agreement concerning inclusion of doctoral thesis in the Institutional Repository of the University of Leiden
Downloaded from:	https://hdl.handle.net/1887/3663612

Note: To cite this publication please use the final published version (if applicable).

CHAPTER 5

Neutralizing antibodies impair the efficacy of reovirus as oncolytic agent but permit effective combination with T-cell-based immunotherapy

Christianne Groeneveldt[1], Priscilla Kinderman[2], Lisa Griffioen[1], Olivia Rensing[2], Camilla Labrie[1], Diana J. M. van den Wollenberg[3], Rob C. Hoeben[3], Matt Coffey[4], Houra Loghmani[4], Els M. E. Verdegaal[1], Marij J. P. Welters[1], Sjoerd H. van der Burg[1], Thorbald van Hall[1] and Nadine van Montfoort[2]

[1] Department of Medical Oncology, Oncode Institute, Leiden University Medical Center, 2333 ZA, Leiden, The Netherlands

[2] Department of Gastroenterology and Hepatology, Leiden University Medical Center, 2333 ZA, Leiden, The Netherlands

[3] Department of Cell and Chemical Biology, Leiden University Medical Center, 2300 RC, Leiden, The Netherlands

[4] Oncolytics Biotech Incorporated, Calgary, AB, Canada

[#] Corresponding author

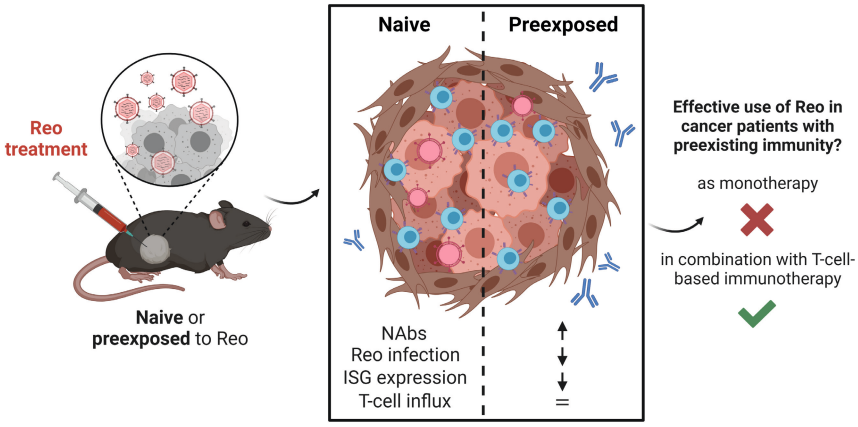
Manuscript submitted

ABSTRACT

Oncolytic reovirus type 3 Dearing (Reo) is an attractive anticancer agent for the treatment of solid tumors. Direct killing of tumor cells (oncolysis) as well as induction of intratumoral T-cell influx contribute to its anticancer efficacy. Since the majority of the human population has been preexposed to Reo, neutralizing antibodies (NAbs) are prevalent in cancer patients and might present a barrier to effective Reo therapy. Here, we confirmed that NAbs are present in the majority of cancer patients and thus investigated the effect of preexposure-induced and therapy-induced NAbs on the anticancer efficacy of Reo therapy in preclinical mouse models. The presence of preexposure-induced NAbs reduced Reo tumor infection and the expression of interferon-stimulated genes in immunocompetent mice and prevented Reo-mediated control of tumor growth. In B-cell deficient mice, the lack of NAbs provided enhanced tumor growth control after Reo monotherapy. Importantly, the intratumoral T-cell influx was not affected by the presence of preexposure-induced or therapy-induced NAbs. Consequently, combinatorial antitumor strategies comprising Reo and T-cell-engagers or checkpoint inhibitors remained effective in these settings. Altogether, our data provide preclinical evidence that NAbs hamper the efficacy of Reo when used as oncolytic agent, but that potent antitumor responses induced by combined Reo and T-cell-based immunotherapy can still be achieved. Given the high prevalence of seropositivity for Reo in cancer patients, these data strongly advocate for the use of Reo as part of a T-cell-based combinatorial approach to unleash its full potential and allow maximal anticancer efficacy, without obstruction by preexisting immune responses.

Synopsis: The presence of neutralizing antibodies hampers the oncolytic function of reovirus, but not its T-cell-attracting capacity. Since the majority of humans has been preexposed to reovirus, this implicates that reovirus should exclusively be used as part of T-cell-based immunotherapeutic strategies to ensure optimal efficacy in cancer patients.

GRAPHICAL ABSTRACT



INTRODUCTION

Oncolytic viruses (OVs) represent a highly promising treatment strategy for a wide range of cancers, by mediating both the direct killing of tumor cells as well as the induction of potent immune responses. These immunostimulatory properties of OVs can be exploited to convert a cold tumor-microenvironment (TME) of solid tumors into a T-cell-infiltrated TME, leading to an increased response to other forms of immunotherapy (1). Oncolytic reovirus type 3 Dearing (Reo) is one of the leading OVs for clinical development (2). In our previous studies using the preclinical murine pancreatic KPC3 tumor model, Reo demonstrated great immunostimulatory potential by inducing a strong interferon response in these tumors, which subsequently attracted a wave of $CD8^+$ T cells. These immunostimulatory characteristics enabled Reo to significantly enhance the efficacy of otherwise unsuccessful CD3-bispecific antibody therapy in these tumors (3).

In the clinic, Reo is often administered intravenously and has demonstrated limited potential when applied as monotherapy (4-6). Although various aspects might contribute to this limited efficacy, one potential barrier to the clinical success of Reo is preexisting immunity against the virus (7). The majority of individuals have acquired preexisting immunity against reovirus after non-symptomatic exposure, indicated by the detection of neutralizing antibodies (NAbs) in patient sera before treatment with Reo (5,8-12). It was demonstrated that Reo can still reach the TME in the presence of NAbs, which was explained by Reo cell carriage via circulating immune cells (13). Since additional studies demonstrated that the uptake and delivery of Reo particles to the tumor via these cellular carriers was enhanced in the presence of NAbs (14,15), this may have led to a common belief that NAbs do not represent a barrier and may even be beneficial for reovirus therapy. But, to the best of our knowledge, a direct comparison of the antitumor efficacy of Reo therapy in settings with and without preexisting NAbs has not been performed.

To this purpose, we developed an experimental setting in immunocompetent mice to study the effect of preexposure- or therapy-induced NAbs on both the oncolytic, as well as the immunostimulatory capacity of Reo. NAbs hampered Reo infection and the Reo-induced expression of interferon-stimulated genes (ISGs), and prevented Reo-mediated control of tumor growth. However, NAbs did not impair the Reo-induced intratumoral T-cell influx and T-cell-based viro-immunotherapeutic combination strategies remained effective, even in the context of clinically preferred intravenous administration. Combined, this study demonstrates that preexisting immunity is detrimental to Reo monotherapy, but Reo can still be employed to sustain effective T-cell-based immunotherapy.

MATERIAL & METHODS

Serum from healthy volunteers and cancer patients

Serum samples from the various cancer patient cohorts were obtained during various Phase I/II studies that were approved by the Medical Ethics Committee of the LUMC, and all patients gave written informed consent before inclusion in the respective studies. The use of serum samples and corresponding geographical data (gender, age) from these cohorts was approved by the LUMC Biobank Review Committee under reference number RP23.023. Patients with recurrent Epithelial Ovarian Cancer from the 'Ovarium Carcinoma' cohort (study number NCT01637532) were treated to evaluate the safety and feasibility of tocilizumab in combination with carboplatin/(pegylated liposomal) doxorubicin and interferon-α2b (Peg-Intron) (16). Patients in the 'Melanoma' cohort (study number P04.085) were treated with adoptive T-cell transfer consisting of tumor-reactive autologous T cells (17). Patients from the 'Cervical Carcinoma' cohort were included in the CIRCLE study investigating cellular immunity against anogenital lesions (18). Patients with metastatic colorectal cancer from the 'Colon Carcinoma' cohort (study number ISRCTN43704292) were enrolled in a phase I/II trial investigating the safety and efficacy of a p53-synthetic long peptide (SLP) vaccine (19). Serum from healthy donors was obtained through the Leiden University Medical Center (LUMC) Voluntary Donor Service (LuVDS, Leiden, The Netherlands) after ethical approval under reference number LuVDS22.049. The age of healthy donors was matched to the age range within the cancer patient cohorts.

Reovirus

The wild-type reovirus strain R124 (here referred to as Reo) was previously isolated from a heterogeneous reovirus Type 3 Dearing (T3D) stock (VR-824) obtained from the American Type Culture Collection (ATCC) by two rounds of plaque purification using HER911 cells (20). All experiments were performed using cesium chloride (CsCl)-purified stocks as described earlier (3). The total amount of particles was calculated based on OD_{260} values where 1 OD equals $2.10x10^{12}$ reovirus particles/mL (21), and the infectious titer was quantified by plaque assay on HER911 cells (22). Clinical-grade Reo (Pelareorep) was provided by Oncolytics Biotech Incorporated (Calgary, AB, Canada).

Cell lines

The murine pancreatic cancer cell line KPC3 (RRID:CVCL_A9ZK) is a low-passage derivate of a primary KPC tumor with mutant *trp53* and *K-ras* from a female C57BL/6 mouse (3,23). KPC3.TRP1 cells (RRID:CVCL_A9ZL) were generated as described (24) and selected for expression of tyrosine-related protein (TRP1) by cell sorting using an αTRP1 antibody (clone: TA99). The MC38 cell line (RRID: CVCL_B288) is a chemically-induced murine colon carcinoma and was obtained from Prof. F. Ossendorp (Leiden University Medical Center, The Netherlands). The human breast cancer cell line BT474 (RRID:CVCL_0179) was purchased from the ATCC (ATCC-HTB-20). KPC3(.TRP1), MC38, and BT474 cells were cultured at 37 °C in a humidified atmosphere containing 5% CO_2

in Iscove's Modified Dulbecco's Medium (IMDM; Gibco) supplemented with 8% fetal calf serum (FCS; Bodinco, Alkmaar, The Netherlands), 2mM L-glutamine (Gibco), 100 U/mL penicillin and 100 µg/mL streptomycin (Gibco). The human embryonic retinoblast cell line HER911 (RRID:CVCL_1K15) was cultured in Dulbecco's Modified Eagle's Medium (DMEM; Gibco), supplemented as described above. The tumor cell line TC1 (RRID:CVCL_4699) expresses the HPV16-derived oncogenes E6 and E7 and activated Ras oncogene and was cultured in IMDM medium as described above but with the addition of 400 µg/ml Geneticin (G418; Life Technologies), 1% nonessential amino acids (Life Technologies), and 1 mM sodium pyruvate (Life Technologies) (25). Cell lines were assured to be free of *Mycoplasma* by regular PCR analysis. The authentication of the cell lines was done by Short Tandem Repeat (STR) profiling (IDEXX BioAnalytics, Ludwigsburg, Germany) and only cells of low passage number were used for experiments.

Antibodies for in vivo administration

The CD3xTRP1 bispecific antibody (bsAb) used is a knob-into-hole bispecific based on murine IgG2a with an Fc Silent™ mutation, featuring one arm with an anti-mouse CD3e scFv based on the clone 145-2C11, and the other arm containing the TA99 clone directed against TRP1 (bAb0136; Absolute Antibody). PD-L1 blockade was performed using a PD-L1-blocking antibody (clone 10F.9G2; GoInVivo™ Purified anti-mouse CD274 Antibody; BioLegend). αCD20 antibodies (clone 18B12) were obtained from Absolute Antibody, and αCD8 (clone 2.43), αCD4 (GK1.5) and αNK1.1 (clone PK136) antibodies were all obtained from BioXcell.

Animal experiments

Male C57BL/6J mice (RRID:IMSR_JAX:000664) (6-8 weeks old) were purchased from Charles River Laboratories (France). Male B6.129S2-Ighm^{tm1Cgn}/J mice (µMT) (RRID:IMSR_JAX:002288) (6-8 weeks old) were purchased from The Jackson Laboratory. Male and female nonobese diabetic (NOD).Cg-Prkdc^{scid}Il2rg^{tm1Wjl}/SzJ (NSG) mice (RRID:IMSR_JAX:005557) (6-16 weeks old) were obtained from The Jackson Laboratory and maintained at the breeding facility of the LUMC in Leiden, The Netherlands. All mouse experiments were individually prepared, reviewed, ethically approved, and registered by the institutional Animal Welfare Body of the LUMC and carried out under project license AVD1160020187004, issued by the competent authority on animal experiments in The Netherlands (named CCD). Experiments were performed following the Dutch Act on Animal Experimentation and EU Directive 2010/63/EU ("On the protection of animals used for scientific purposes") at the animal facility of the LUMC. Mice were housed in individually ventilated cages with no more than 5 mice/cage and experiments were initiated after one week of acclimatization after transport.

For preexposure, mice were injected intravenously with 10^7 plaque-forming units (pfu) of Reo in a volume of 100 µL phosphate-buffered saline (PBS, Fresenius Kabi) at two consecutive times with a 2-week interval. In depletion experiments, depletion using αCD20, αNK, αCD8, or αCD4 antibodies (100 µg in 100 µL PBS, intraperitoneally (i.p.))

was initiated 5 and 2 days before the first Reo preexposure, and hereafter depletion was maintained by weekly injections until indicated. Alternatively, αCD4 injections were initiated before the second Reo preexposure or before tumor challenge. Depletion of designated cell populations was verified by flow cytometry before mice received further interventions.

After preexposure or at the start of the experiment, mice were inoculated in the right flank with subcutaneous KPC3(.TRP1) tumors ($1x10^5$ cells in 100 µL PBS/0.1% bovine serum albumin (BSA, Sigma-Aldrich) or MC38 tumors ($5x10^5$ cells in 200 µL PBS/0.1% BSA). BT474 tumors were orthotopically engrafted by injecting $5x10^6$ cells in a volume of 100 µL 1:1 (v/v) PBS/0.1% BSA : Growth Factor Reduced matrigel (Corning®) in the fourth mammary fat pad of isoflurane-anesthetized female NSG mice. Mice with palpable tumors were allocated into groups with similar average tumor volumes and assigned a treatment regimen. Intratumoral Reo administration was performed under isoflurane anesthesia by injection of 10^7 pfu of Reo or PBS as a control in a volume of 30 µL on 3 consecutive days unless otherwise indicated. Intravenous Pelareorep administration was performed by injection of $2x10^8$ pfu of Pelareorep in a volume of 100 µL PBS in the tail vein on indicated days, with 5-day intervals. Treatment with CD3xTRP1 bsAbs consisted of 3 i.p. injections of 12.5 µg antibody in 100 µL PBS, given every other day or with 5-day intervals. αPD-L1 antibodies were administered on indicated days by i.p. injection of 200 µg antibody in 100 µL PBS.

Cages were randomly allocated to a certain treatment group by an independent researcher and treatments were given in a different order each time. During all experiments, tumor size and/or body weight were measured 3 times a week in 3 dimensions using a caliper, in a blinded manner concerning preexposure status, genotype, or depletion group when possible. Blood was collected in lithium heparin-coated microvettes (Sarstedt) from the tail vein on indicated days for interim analysis of immune cells. Plasma was obtained by centrifugation (14.000 rpm, 15 min, 4 °C) and stored at -80 °C for assessment of neutralizing antibodies. For tumor growth experiments, mice were sacrificed when the tumor volume exceeded 1000 mm^3 or when ulceration occurred. Therapy response was determined as follows: NR = no response; CR = complete response and PR = partial response (regression or constant tumor volumes for at least 7 days). For intratumoral analysis experiments, mice were sacrificed at indicated days after treatment, and tumors, spleens, tumor-draining lymph nodes (TDLN), and blood were collected. Tumors were divided into representative parts, which were either snap-frozen in liquid N2 and stored at -80 °C until further analysis, fixed in 4% formaldehyde (AddedPharma) for immunohistochemistry or immediately processed to single cells suspensions to analyze the cellular composition by flow cytometry.

Neutralization assay

HER911 cells were seeded in flat-bottom 96-well plates in a density of $1x10^4$ cells/well and allowed to adhere overnight in the incubator (37 °C, 5% CO_2, 90% humidity). The next day, human serum samples or murine plasma samples were heat-inactivated by incubation at 56 °C for 30 minutes. For human serum samples, a two-fold dilution series (starting with 1:5) was prepared in DMEM with 2% FCS. Nanogam® (Sanquin, Amsterdam, The Netherlands), a pool of immunoglobulins of >1000 donors, was used as a positive control. For murine plasma samples, a 2-fold or 4-fold dilution series was prepared (starting with 1:25, 1:50, or 1:100) in DMEM with 2% FCS. Serum or plasma samples were mixed with 150 pfu/well of Reo and incubated for 30 minutes at 37 °C to allow the binding of NAbs to Reo particles. Next, the serum/plasma:Reo samples were transferred in duplo onto the HER911 cells. Cell growth was determined at 3 days post-infection by crystal violet staining. In short, cells were fixed with ice-cold methanol (Merck) for 10 minutes at -20 °C. Hereafter, cells were incubated with 0.5% crystal violet (Sigma-Aldrich) in 20% methanol for 20 minutes at room temperature (RT). Plates were extensively washed with H_2O and air dried. After drying, plates were incubated with 100 uL of methanol for 20 minutes at RT before measuring the optical density (OD) at 570 nm using a SpectraMax iD3 multi-mode plate reader (Molecular Devices). The measured OD_{570} value of the positive (Reo only) control was set to 100% and that of the negative (medium only) control to 0%. The OD_{570} of the samples were normalized using these controls and IC_{50} values were calculated using nonlinear regression analysis and sera with IC_{50} < 10 were regarded as negative.

Cell preparation and flow cytometry

Tumors were minced in small pieces and incubated with Liberase TL (Roche) for 15 minutes at 37 °C. The reaction was stopped by the addition of culture medium with 8% FCS and the mixture was gently dissociated into a single-cell suspension over a cell strainer (Corning). Spleens and TDLNs were dissociated into a single-cell suspension over a cell strainer. Blood and splenocytes were incubated with lysis buffer (Pharmacy LUMC) for 3 minutes at RT to remove all red blood cells before use. Cells were incubated with Zombie AquaTM Fixable Viability Dye (BioLegend) in PBS for 20 minutes at RT followed by incubation with 2.4G2 FcR blocking antibodies (clone 2.4G2; BD Biosciences) in FACS buffer (PBS, 0.5% BSA, and 1% sodium azide) for 20 minutes on ice. If applicable, cells were incubated with Reo $\mu1_{133\text{-}140}$ tetramer (Tm) conjugated to APC or the Reo $\mu1_{422\text{-}430}$ Tm conjugated to PE (both generated *in-house*) for 1 hour at RT in FACS buffer, after which surface markers (**Table S1**) were added directly to the tetramer mixture and incubated for 30 minutes at RT. After completion of the staining protocol, samples were fixed in 1% paraformaldehyde (Pharmacy LUMC) and acquired using a BD LSRFortessa™ X20 4L cell analyzer (BD Biosciences, San Jose, CA, USA) at the Flow cytometry Core Facility (FCF) of the LUMC (https://www.lumc.nl/research/facilities/fcf). Data were analyzed using FlowJo™ Software Version 10 (Becton, Dickinson, and Company). Opt-SNE plots (26) were generated using standard settings in OMIQ data analysis software (Omiq, Inc. www.omiq.ai).

Intracellular cytokine staining

Ex vivo tumor single-cell suspensions were cocultured with Reo-infected TC1 cells (MOI 10) or Reo-derived peptides (1 µg/mL) to assess recognition. Sequences of Reo-derived peptides (**Table S2**) were obtained from a study by Murphy *et al* where the MHC-I ligandome of Reo-infected ovarian surface epithelial cells (ID8; H2-K^b/H2-D^b) was investigated using comparative mass spectrometry (27). Identified Reo-derived peptides were ordered as a micro-scale crude peptide library (GenScript, Leiden, The Netherlands). Effector cells and target cells or peptides were cocultured for 6 hours in the presence of BD GolgiPlug™ (BD Biosciences). PMA (20 ng/mL) and ionomycin (1 µg/mL) were used as a positive control. After incubation, cells were washed and stained for CD8α (clone 53-6.7; BioLegend). Thereafter, cells were fixed with Fixation Buffer (BioLegend) according to the manufacturer's instructions, followed by staining for intracellular IFNγ (clone XMG1.2; BioLegend). After completion of the staining protocol, samples were fixed in 1% paraformaldehyde and acquired using the BD LSRFortessa™ X20 4L cell analyzer.

Western blotting

The presence of antibodies against Reo proteins in the plasma of naive or preexposed mice was investigated by Western blotting. HER911 cells were infected with reovirus (multiplicity of infection = 10) for 24 hours, after which cells were lysed in radioimmunoprecipitation assay (RIPA) buffer (Bioke) containing protease and phosphatase inhibitors (ThermoFisher Scientific). Proteins (10-15 µg) were separated on a 4-15% mini-protean TGX gel (Bio-Rad) and then transferred to a 0.2 µM nitrocellulose membrane (Bio-Rad). After blocking for 1 hour at RT with Pierce™ Protein-Free Blocking Buffer (ThermoFisher Scientific), the membrane was incubated overnight at 4°C with pooled plasma from preexposed or naive mice (n=5-6) (1:200). As a positive control, the membrane was incubated with anti-µ1 (clone 10F6; Developmental Studies Hybridoma Bank, 1:200). The next day, membranes were incubated with horseradish peroxidase (HRP)-conjugated goat anti-mouse IgG+IgM+IgA (Abcam, 1:1000) at RT for 1 hour. Proteins were detected on the Chemidoc imaging XRS+ system (Bio-Rad) using the Clarity Western ECL Substrate kit (Bio-Rad).

RNA isolation and RT-qPCR

A representative snap-frozen proportion (10-30 mg) of each tumor or organ was disrupted in lysis buffer (Promega) using a stainless bead and the TissueLyser LT (Qiagen). Total RNA of tumor samples was isolated using the ReliaPrep™ RNA Tissue Miniprep System (Promega) according to the manufacturer's protocol. 500 ng of RNA was used to generate cDNA using the High-Capacity RNA-to-cDNA™ Kit (ThermoFisher Scientific) according to the manufacturer's protocol. Reo genomic copies and expression levels of host genes (**Table S3**) in tumors were measured by RT-qPCR as previously described (3). Reo S4 copy numbers were determined based on a standard curve, generated with serial dilutions of plasmid pcDNA_S4. Log_{10} S4 copy numbers were calculated using a previously described formula (28). The expression of host genes

was normalized to reference genes *Mzt2* and *Ptp4a2* using the Bio-Rad CFX Manager 3.1 Software (Bio-Rad).

Immunohistochemistry

Formaldehyde-fixed, paraffin-embedded tissue sections were stained for cleaved caspase-3. Formalin-fixed tumor pieces were embedded in paraffin and then sectioned randomly at 4 µm and placed on Superfrost® Plus slides (VWR). Sections were dried overnight at 37 °C and stored at 4 °C until staining. Slides were deparaffinized and endogenous peroxidase was blocked with 0.3% hydrogen peroxidase (VWR) in methanol for 20 minutes. After rehydration, antigen retrieval was performed by boiling slides for 10 minutes in 0.01M sodium citrate (pH=6.0; Merck). Non-specific binding was blocked using SuperBlock™ (ThermoFisher Scientific) before overnight incubation at 4 °C with rabbit anti-mouse cleaved caspase-3 antibody (clone Asp175, 1:400; Cell Signaling Technology). Hereafter, slides were incubated for 30 min at RT with a biotinylated goat anti-rabbit secondary antibody (1:200; Agilent), followed by incubation with avidin-biotin complex (VECTASTAIN® Elite® ABC HRP Kit; Vector Laboratories). Peroxidase activity was detected using the 2-component liquid DAB+ system (Agilent) according to the manufacturer's instructions for 5 min. Slides were counterstained with hematoxylin (Sigma-Aldrich), dehydrated, and mounted using Entellan (Sigma-Aldrich). Control sections were processed in parallel but without incubation with the primary antibody. No labeling was observed in the control sections.

IFNγ ELISA

Sorted Reo $\mu1_{133\text{-}140}$ Tm^+ or Reo $\mu1_{422\text{-}430}$ Tm^+ cells (2000 cells/well of a round-bottom 96-wells plate) were cocultured with PMA (20 ng/mL) and ionomycin (1 µg/mL), Reo-infected TC1 cells (20.000 cells/well) or Reo-infected TC1 cells. In some wells, NAb-containing plasma from Reo-preexposed mice (1:1000 dilution) was added. After 48 hours of incubation, supernatants were harvested. For ELISA, Nunc MaxiSorp™ plates (Corning) were coated with purified rat anti-mouse IFNγ antibody (BD Pharmingen) in sodium carbonate/sodium bicarbonate coating buffer (pH 9.6) overnight at 4 °C and then blocked with PBS/1% BSA/0.05% Tween-20 (Merck) for 1 hour at 37 °C. After washing with wash buffer (PBS/0.05% Tween-20), 100 µL of supernatant was added and incubated for 2 hours at RT. The standard curve was prepared using recombinant mouse IFNγ (BioLegend). After washing, biotinylated rat anti-mouse IFNγ antibody (BD Pharmingen) was applied for 1 hour at RT, followed by poly-Streptavidin-HRP conjugate (Sanquin, The Netherlands) for 1 hour at RT. After washing, 50 µL of TMB (3,3',5,5'-Tetramethylbenzidine) (Sigma-Aldrich) was added and the reaction was quenched by the addition of 50 µL 2M H_2SO_4 (Merck). Absorbance was measured at 450 nm using a SpectraMax iD3 multi-mode plate reader (Molecular Devices).

Statistics

Group size was calculated using the PS: Power and Sample Size Calculation program (Vanderbilt University, version 3.1.6) (29). For experiments where tumor growth was the experimental read-out, mice were excluded when tumor engraftment was not successful (1% of all tumor engraftments). For RT-qPCR analysis, samples were excluded when RNA concentration and purity were too low (< 75 ng/µL). For flow cytometry data, tumor samples were excluded when macroscopic evidence for draining lymph node contamination was present.

All graphs were prepared and statistical analyses were performed using the GraphPad Prism software (version 8). All data represent mean±SEM and key observations are based upon multiple experiments with similar results. For the comparison of two groups, an unpaired t test was used. For comparing multiple groups versus PBS treatment or negative control, an one-way analysis of variance (ANOVA) including Dunnett's post hoc test was performed. For comparing multiple groups with each other, an one-way ANOVA including Tukey's post hoc test was used. To compare differences in average tumor growth, an ordinary two-way ANOVA with Tukey's post hoc test was used. IC50 values were calculated using non-linear regression analysis. Survival between groups was compared using Kaplan-Meier curves and the statistical Log-rank test (Mantel-Cox). More information regarding the statistical tests used can be found in the individual figure legends. Significance levels are labeled with asterisks, with *p<0.05, **p<0.01, ***p<0.001, and ****p<0.0001. Non-significant differences are indicated by ns.

RESULTS

Preexisting immunity against Reo is prevalent in the human population

The use of oncolytic reovirus type 3 Dearing (hereafter named Reo) is an emerging anticancer treatment and a promising strategy to enhance the efficacy of immunotherapy. However, various factors, including the presence of preexisting neutralizing antibodies (NAbs) might limit its anticancer potential. Before investigating the effect of preexisting immunity on various aspects of Reo therapy, we determined the level of seropositivity against Reo in healthy volunteers and various cohorts of cancer patients. Using serial dilutions of serum in a virus neutralization assay, we observed that 81.0% of all tested individuals (n=100) carried Reo-specific NAbs (**Figure 1A, B**). The frequency of seropositivity did not differ between healthy volunteers and cancer patients (**Figure 1C**), or between male and female individuals (**Figure 1D**). Reo is known as a 'kindergarten' virus and higher seropositivity might thus be expected in younger individuals, but the level of seropositivity was not correlated with age (**Figure 1E**). Combined, these data confirm that the majority of the human population has been preexposed to Reo, which underscores the relevance to determine the effect of preexposure on the efficacy of Reo-based anticancer therapies.

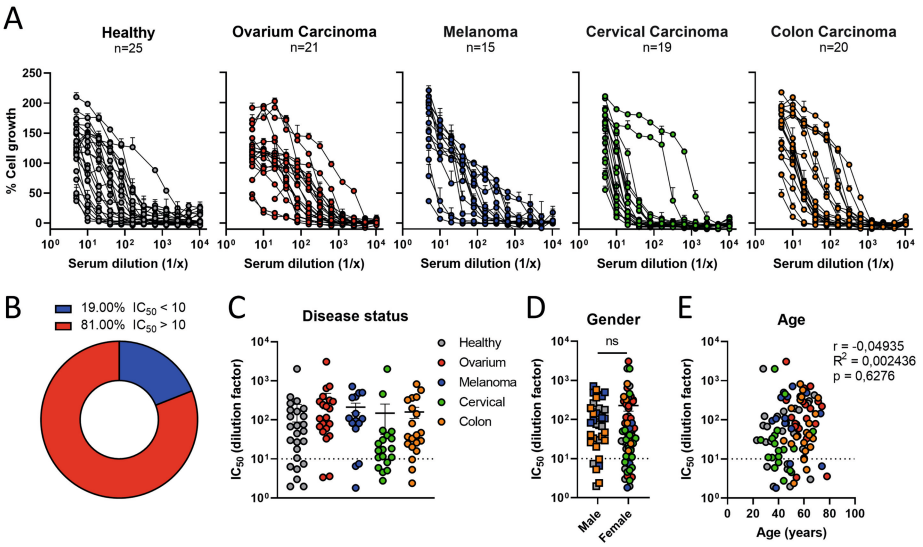


Figure 1. Preexisting immunity against Reo is prevalent in the human population. (**A**) Individual serum samples from healthy volunteers or cancer patients with different primary tumors were subjected to a Reo neutralization assay. Percentage of cell growth is calculated by normalizing for Reo only (0% viable) and Mock (100% viable). (**B**) Percentage of all individuals that tested seropositive (IC_{50} > 10) or seronegative (IC_{50} < 10) for Reo. (**C**) Comparison of IC_{50} values between healthy volunteers and cancer patient cohorts. (**D**) Comparison of IC_{50} values between male and female individuals. (**E**) Correlation analysis between IC_{50} values of individuals and corresponding age in years. Data represent mean±SEM. IC_{50} values were calculated using non-linear regression analysis. Differences between groups in (C) were determined using a Kruskal-Wallis test with Dunn's multiple comparisons test. Differences between groups in (D) were determined using an unpaired t test with Welch's correction, and correlation between IC_{50} values and age in (E) was determined by calculating the Pearson correlation coefficient (r). Significance levels: ns=not significant.

Preexposure impairs intratumoral Reo infection and the Reo-induced interferon response

To study the role of preexisting immunity on Reo antitumor efficacy, we established an experimental model where immunocompetent C57BL/6J mice were preexposed to Reo with a two-week interval (**Figure 2A**). This preexposure led to the presence of high levels of NAbs in the circulation (**Figure 2B, C**), as well as $CD8^+$ T cells recognizing the Reo $\mu1_{133\text{-}140}$ epitope that we identified earlier (**Figure 2D**) (30). These NAb levels remained high over time (**Figure S1**). Western blot analysis using the plasma of preexposed mice as the primary antibody source revealed that Reo-specific antibodies also predominantly recognize the μ1 protein (**Figure 2E**), suggesting that immunodominant Reo-specific T-cell and B-cell responses are both directed to the same viral protein.

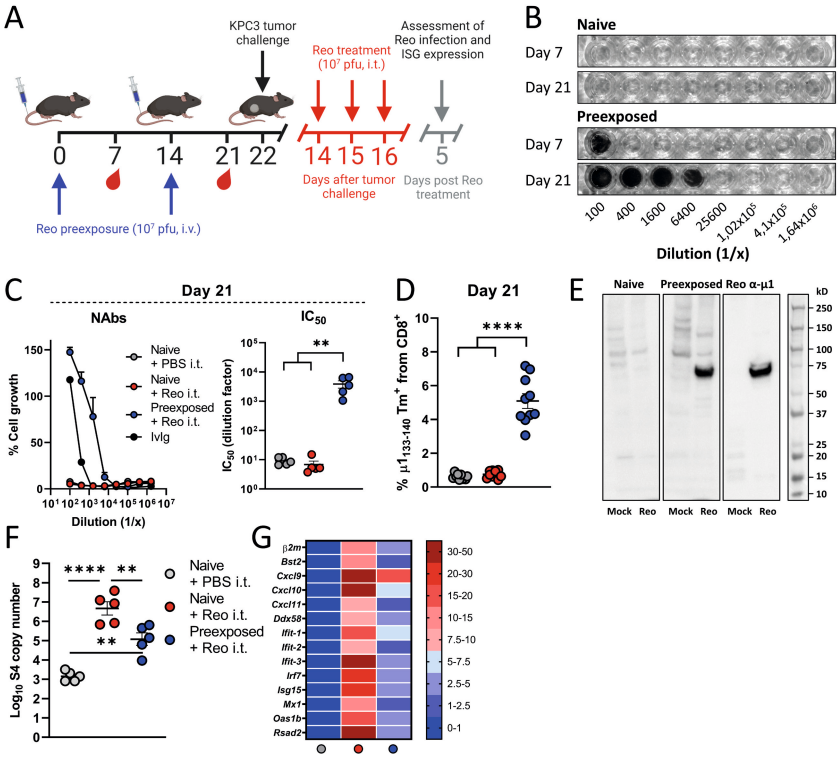


Figure 2. Preexposure impairs Reo infection and the Reo-induced interferon response. (**A**) Overview of experiment described in (B-G). Male C57BL/6J mice (n=5/group) were preexposed by intravenous (i.v.) injection of Reo (10^7 plaque-forming units (pfu)/injection) on days 0 and 14. Blood was drawn on days 7 and 21 for interim analysis. After preexposure, mice were subcutaneously inoculated with KPC3 cells ($1x10^5$/mouse) and received intratumoral (i.t.) Reo injections (10^7 pfu/injection) on indicated days. Tumors were harvested 5 days after Reo administration for *ex vivo* analysis. (**B**) Representative pictures of crystal violet-stained 911 cells after subjection to a neutralization assay with diluted plasma from naive or preexposed mice. (**C**) Reo neutralization assay. Average dilution curves using plasma from naive or preexposed mice and individual IC_{50} values on day 21. (**D**) Frequency of Reo-specific $\mu1_{133-140}$ tetramer $(Tm)^+$ $CD8^+$ T cells in the circulation on day 21. (**E**) Western blot of Mock or Reo-infected 911 cell lysates using antibodies against the Reo μ1 protein or plasma of preexposed mice as primary antibody source. (**F**) Intratumoral presence of genomic copies of Reo S4 segment, as measured by quantitative reverse transcription PCR (RT-qPCR). (**G**) Heatmap depicting relative expression of various interferon response genes on day 5, as determined by RT-qPCR on bulk tumor RNA. Data represent mean±SEM. IC_{50} values were calculated using non-linear regression analysis. Differences between groups in (C), (D), and (F) were determined using an ordinary one-way analysis of variance (ANOVA) with Tukey's post hoc test. Significance levels: **p<0.01 and ****p<0.0001.

As a first step of Reo anticancer efficacy, we investigated whether Reo infection of the tumor was affected by preexisting immunity. After preexposure, mice were engrafted with KPC3 tumors and received intratumoral Reo injections when tumors were palpable. On day 5 post Reo treatment, mice were sacrificed for intratumoral analysis. Importantly, the quantity of intratumoral genomic copies of the Reo S4 segment was significantly decreased in preexposed mice compared to naive mice, implying impaired viral infection (**Figure 2F**). Concomitantly, the expression of a panel of interferon-stimulated genes

(ISGs), such as *Ifit-1, Ifit-2,* and *Ifit-3*, as well as T-cell attracting chemokines *Cxcl10* and *Cxcl11*, was lower in tumors of preexposed mice (**Figure 2G**). Of note, the expression of chemokine *Cxcl9* appeared to be less affected. Altogether, we concluded that Reo preexposure is associated with a strong decrease in Reo genomic copies and ISG expression in tumors upon Reo treatment.

Reo-specific NAbs impair the anticancer efficacy of Reo monotherapy

We next specifically investigated the effect of NAbs after Reo preexposure. μMT mice, which lack B cells and thus cannot produce antibodies (**Figure S2A-D**), were exposed to Reo but succumbed to weight loss (**Figure S2E**) two weeks after inoculation, suggesting that Reo replication was uncontrolled in the absence of NAbs. Then, a tumor challenge experiment was performed in a small number of immunocompromised NSG mice that are also B-cell deficient. Similarly, Reo-exposed NSG mice succumbed to weight loss, and high numbers of Reo genomic copies were detected in tumors, livers, hearts, and plasma of these mice, indicating viremia in the absence of NAbs (**Figure S2F-I**). These data and similar observations by others (31-33) demonstrate that NAbs are necessary to prevent uncontrolled Reo infection in mice.

We then investigated the effect of strongly decreased, but not completely absent, levels of NAbs on Reo infection in immunocompetent C57BL/6J mice by injection of αCD20 antibodies to deplete B cells (**Figure 3A**). Indeed, although the depletion of B cells was efficient in blood (**Figure S3A, B**), neutralization assay (**Figure 3B**) and Western blot analysis (**Figure S4**) showed that residual levels of NAbs were still present in the plasma of preexposed mice. These low NAb levels were sufficient to protect mice from Reo-induced pathology but, importantly, hampered Reo infection (**Figure 3C**) and ISG expression (**Figure 3D**) in the tumor. Even the intratumoral administration of a 10-fold higher dose of Reo to preexposed mice did not increase the presence of genomic Reo S4 copies (**Figure 3D**), demonstrating that even low systemic levels of NAbs significantly hamper intratumoral Reo infection and ISG expression. This suggests that achieving effective infection in most patients will be difficult, including those with low NAb levels.

Due to the crucial role of $CD4^+$ T cells in establishing effective class-switched B-cell responses, we depleted $CD4^+$ T cells during Reo preexposure as another way to influence NAbs (**Figure 3E, S3C, D**). Depletion of $CD4^+$ T cells during preexposure, but not $CD8^+$ T cells or NK cells, completely abrogated NAb production (**Figure 3F**) and significantly increased genomic Reo S4 copies (**Figure 3G**) and the expression of ISGs (**Figure 3H**) in the tumor upon intratumoral Reo treatment. Combined, these data clearly show that the presence of Reo-specific NAbs impairs infection and ISG expression, even when Reo is injected directly into tumors.

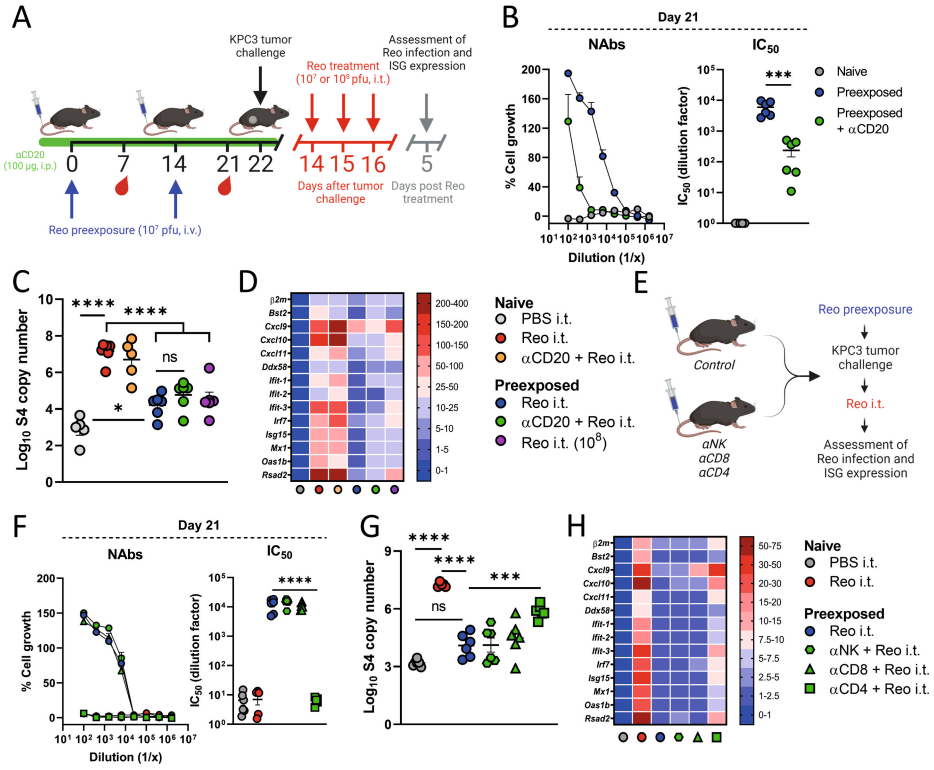


Figure 3. Preexposure-induced Reo-specific NAbs impair Reo infection and ISG expression in the tumor. (**A**) Overview of experiment described in (B-D). Male C57BL/6J mice (n=5-7/group) were preexposed by intravenous (i.v.) injection of Reo (10^7 plaque-forming units (pfu)/injection) on days 0 and 14. Depletion of B cells (**α**CD20, 100 **μ**g/injection, intraperitoneally (i.p.)) was initiated on days -5 and -2 and maintained weekly during the preexposure period. Blood was drawn on days 7 and 21 for interim analysis. After preexposure, mice were subcutaneously inoculated with KPC3 cells (1x10^5/mouse) and received intratumoral (i.t.) Reo injections (10^7 of 10^8 pfu/injection) on indicated days. Tumors were harvested 5 days after Reo administration for *ex vivo* analysis. (**B**) Reo neutralization assay. Average dilution curves using plasma from indicated groups and individual IC_{50} values on day 21. (**C**) Intratumoral presence of genomic copies of Reo S4 segment, as measured by quantitative reverse transcription PCR (RT-qPCR). (**D**) Heatmap depicting relative expression of various interferon response genes on day 5, as determined by RT-qPCR. (**E**) Design of experiment described in (F-H). Experiment was executed exactly as described in (A), but male C57BL/6J mice (n=6/group) received **α**NK, **α**CD8, or **α**CD4 (100 **μ**g/injection, i.p.) during the preexposure period. (**F**) Reo neutralization assay. Average dilution curves using plasma from indicated groups and individual IC_{50} values on day 21. (**G**) Intratumoral presence of genomic copies of Reo S4 segment, as measured by RT-qPCR. (**H**) Heatmap depicting relative expression of various interferon response genes on day 5, as determined by RT-qPCR. Data represent mean±SEM. IC_{50} values were calculated using non-linear regression analysis. To determine differences between groups in (B), (D), and (F), an ordinary one-way analysis of variance (ANOVA) with Tukey's post hoc test was used. Significance levels: ns=not significant, *p<0.05, ***p<0.001, and ****p<0.0001.

Since circulating NAbs can already be detected five days after intratumoral Reo administration (**Figure S5**), these therapy-induced NAbs might hinder the therapeutic potency of intratumoral Reo treatment already at early time points. Therefore, we next evaluated the therapeutic potency of oncolytic Reo in the absence of NAbs in KPC3-bearing B-cell deficient μMT mice (**Figure 4A**). Intratumoral injection with Reo created a therapeutic time window that allowed us to study the role of treatment-induced NAbs before the loss of bodyweight occurred (**Figure 4B**). Reo treatment in μMT mice was associated with significant decreases in tumor volumes, which were not observed in fully immunocompetent, Reo-treated C57BL/6J mice (**Figure 4C**). Similar levels of Reo S4 copies could be found in Reo-treated tumors from μMT mice and C57BL/6J mice, even though tumors from μMT mice were smaller in size (**Figure 4D**). Additionally, the expression of ISGs (**Figure 4E**) and the level of apoptosis, measured by cleaved caspase-3, was higher in tumors of Reo-treated μMT mice compared to those of Reo-treated C57BL/6J mice (**Figure 4F, G**).

To indisputably prove that NAbs impair the antitumor effect of Reo therapy, a NAb transfer experiment was performed. KPC3-bearing NSG mice received naive plasma or NAb-containing plasma from preexposed C57BL/6J mice, at 2 different doses, and subsequently were treated intratumorally with Reo (**Figure 4H, S6**). Even though NAbs were only detected after infusion of the high dose NAb-containing plasma (**Figure 4I**) and NAbs did not reduce the genomic Reo S4 copies in tumors (**Figure 4J**), the transfer of both doses of NAbs reduced the Reo-induced expression of ISGs (**Figure 4K**) and the level of cleaved caspase-3 (**Figure 4L, M**) in the tumor. Importantly, the transfer of NAb-containing plasma, but not naive plasma, completely neutralized the Reo-induced antitumor effect (**Figure 4N**). These combined results show that Reo can have profound antitumor efficacy, but its use as an oncolytic agent is impaired by the presence of NAbs, even at low levels.

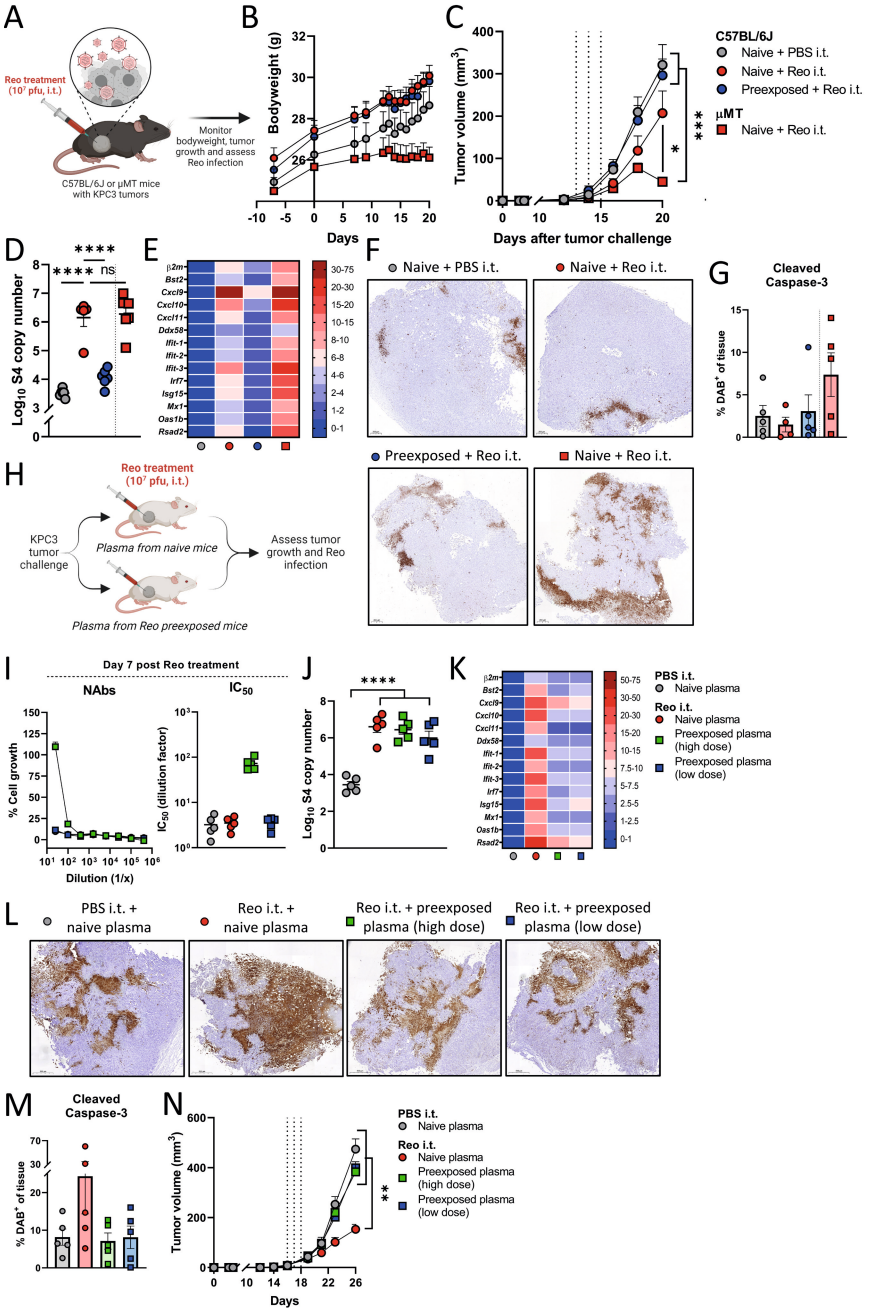


Figure 4. Reo-specific NAbs abrogate the antitumor efficacy of Reo monotherapy. (**A**) Overview of experiment described in (B-G). Male C57BL/6J or µMT mice (n=6/group) were subcutaneously inoculated with KPC3 cells (1x10^5/mouse) and received intratumoral (i.t.) Reo injections (10^7 pfu/injection) on days 13-15. Mice were sacrificed 7 days after Reo administration for *ex vivo* analysis. (**B**) Average bodyweight curves. (**C**) Average tumor volume curves. (**D**) Intratumoral presence of genomic copies of Reo S4 segment, as measured by quantitative reverse transcription PCR (RT-qPCR). >>

>> (**E**) Heatmap depicting relative expression of various interferon response genes, as determined by RT-qPCR. (**F**) Representative images obtained from immunohistochemical staining of KPC3 tumors for apoptosis marker cleaved caspase-3. Scale bar equals 200 µm. (**G**) Quantification of positive DAB signal in sections stained for cleaved caspase-3. (**H**) Overview of experiment described in (I-N). Male and female NSG mice (n=5/group) were subcutaneously inoculated with KPC3 cells ($1x10^5$/mouse) and received intratumoral (i.t.) Reo injections (10^7 pfu/injection) on days 16-18. Plasma from preexposed C57BL/6J mice was injected i.p., 2x/week. Mice were sacrificed 10 days after Reo administration for *ex vivo* analysis. (**I**) Reo neutralization assay. Average dilution curves and individual IC_{50} values using plasma from indicated groups, harvested on day 7 after i.t. Reo administration. (**J**) Intratumoral presence of genomic copies of Reo S4 segment, as measured by quantitative reverse transcription PCR (RT-qPCR). (**K**) Heatmap depicting relative expression of various interferon response genes in tumors, as determined by RT-qPCR. (**L**) Representative images obtained from immunohistochemical staining of KPC3 tumors for apoptosis marker cleaved caspase-3. Scale bar equals 500 µm. (**M**) Quantification of positive DAB signal in sections stained for cleaved caspase-3. (**N**) Average tumor volume curves. Data represent mean±SEM. IC_{50} values were calculated using non-linear regression analysis. Differences between groups in (C) and (N) were determined using an ordinary two-way analysis of variance (ANOVA) with Tukey's post hoc test, and an ordinary one-way ANOVA with Tukey's post hoc test was used to determine differences between groups in (D) and (J). Significance levels: ns=not significant, *p<0.05, **p<0.01, ***p<0.001, and ****p<0.0001.

Preexposure does not affect the Reo-induced intratumoral influx or activation of T cells

Current clinical efforts aim to use Reo not solely as an oncolytic agent, but rather as an immune-stimulatory agent, especially to induce the intratumoral influx of T cells that can be harnessed by T-cell-based immunotherapeutic strategies (34-36). Therefore, we next studied whether the Reo-induced intratumoral T-cell influx therapy is affected by Reo preexposure. Immunocompetent C57BL/6J mice were preexposed to Reo, engrafted with KPC3 tumors, and the frequency, specificity, and effector function of intratumoral T cells after intratumoral Reo treatment were analyzed (**Figure 5A**). Interestingly, the Reo-induced influx of $CD8^+$ T cells was not affected (**Figure 5B, C**). Equally, the intratumoral influx of $CD8^+$ T cells did not differ between Reo-treated µMT mice and Reo-treated C57BL/6J mice, demonstrating that T-cell influx is not affected by the presence or absence of NAbs (**Figure S7A, B**). This might be related to the moderate expression of *Cxcl9* that is still present in tumors of preexposed mice. Of note, the Reo-induced influx of NK cells was lower in preexposed C57BL/6J mice and higher in Reo-treated µMT mice, suggesting that the influx of NK cells is more influenced by the presence of NAbs or ISG expression than the influx of T cells (**Figure 5D, S7C**).

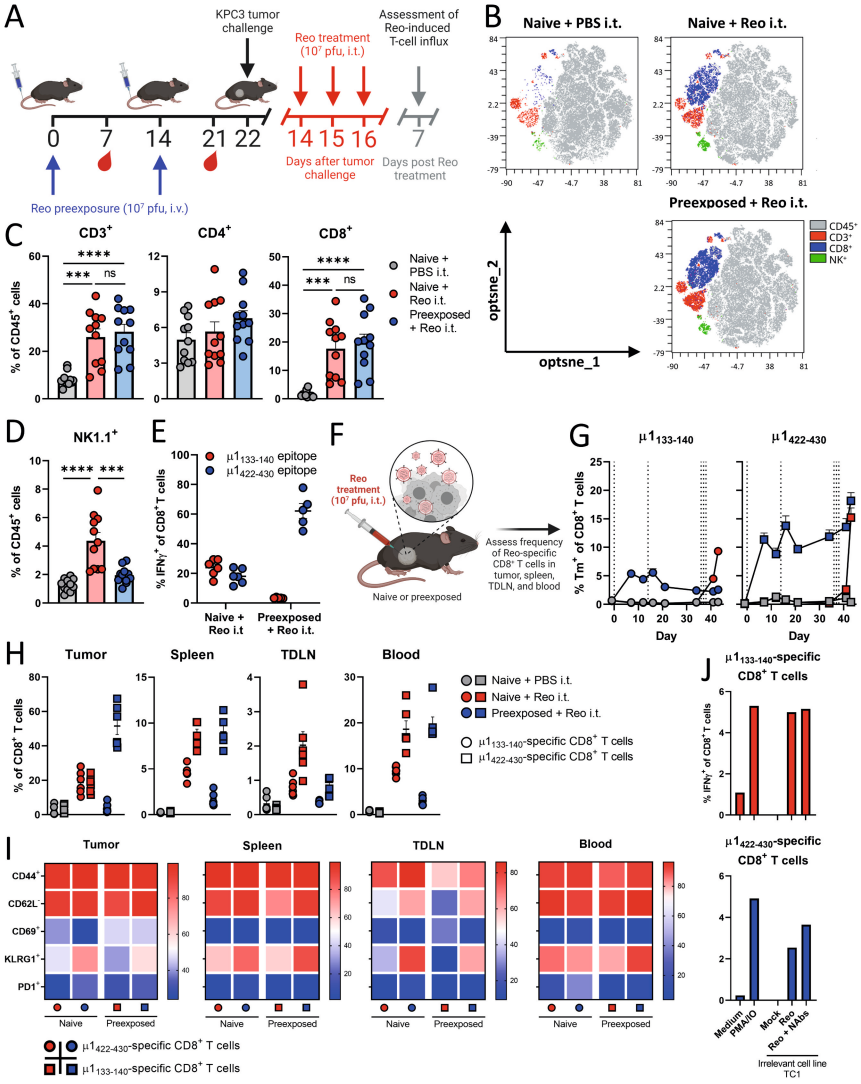


Figure 5. Preexposure does not affect the Reo-induced intratumoral influx or activation of T cells but shifts the frequency of Reo-specific T-cell populations. (**A**) Overview of experiment described in (B-E). Male C57BL/6J mice (n=5-6/group) were preexposed by intravenous (i.v.) injection of Reo (10^7 plaque-forming units (pfu)/injection) on days 0 and 14. After preexposure, mice were subcutaneously inoculated with KPC3 cells ($1x10^5$/mouse) and received intratumoral (i.t.) Reo injections (10^7 pfu/injection) on days 14-16. Tumors were harvested 7 days after Reo administration for *ex vivo* analysis. (**B**) Opt-SNE plots highlighting the intratumoral presence of $CD3^+$, $CD8^+$ T cells, and NK cells after indicated treatments. $1x10^5$ $CD45^+$ cells were subsampled from each sample. (**C**) Intratumoral frequency of $CD3^+$, $CD4^+$, and $CD8^+$ T cells within $CD45^+$ immune cells. (**D**) Intratumoral frequency of NK cells within $CD45^+$ immune cells. (**E**) Frequency of interferon gamma $(IFN\gamma)^+$ cells within the intratumoral $CD8^+$ T-cell population after coculture with indicated peptides, as measured with intracellular cytokine staining. (**F**) Design of experiment described in (G-J). Mice (n=6/group) were preexposed with Reo, inoculated with KPC3 cells, and treated i.t. with Reo as described in (A). (**G**) Kinetics of Reo-specific $\mu1_{133-140}$ and $\mu1_{422-430}$ tetramer $(Tm)^+$ $CD8^+$ T cells in the circulation. (**H**) Frequency of Reo-specific $\mu1_{133-140}$ and $\mu1_{422-430}$ Tm^+ $CD8^+$ T cells in tumor, spleen, tumor-draining lymph node (TDLN), or blood of naive or preexposed mice after intratumoral Reo administration.

>>

>> (**I**) Heatmap showing activation profile of Reo-specific $\mu1_{133-140}$ and $\mu1_{422-430}$ Tm^+ $CD8^+$ T cells in tumor, spleen, TDLN, or blood. (**J**) Production of IFNγ by sorted Reo-specific $\mu1_{133-140}$ or $\mu1_{422-430}$ Tm^+ $CD8^+$ T cells after coculture with indicated targets for 48 hours. Data represent mean±SEM, except in (J) where n=1. In (C) and (D), data from two experiments with the same set-up are pooled and differences between groups were determined using an ordinary one-way analysis of variance (ANOVA) with Tukey's post hoc test. Significance levels: ns=not significant, ***p<0.001, and ****p<0.0001.

Although the intratumoral influx of $CD8^+$ T cells was not affected by the presence of NAbs, the proportion of T cells recognizing our previously identified Reo $\mu1_{133-140}$ epitope was strongly diminished (**Figure S8A**). Intratumoral $CD8^+$ T cells in preexposed mice were still Reo-specific (**Figure S8B**) but now recognized another epitope ($\mu1_{422-430}$) (**Figure 5E, S8C, D**). Further analysis of these two Reo-specific $CD8^+$ T-cell populations using tetramers (**Figure 5F**), revealed different kinetics (**Figure 5G**) and confirmed that especially in tumors of preexposed mice, the frequency of $\mu1_{422-430}$-specific $CD8^+$ T cells dominated over the frequency of those recognizing the $\mu1_{133-140}$ epitope (**Figure 5H**). Both Reo-specific $CD8^+$ T-cell populations exhibited a similar effector phenotype which did not differ between Reo-treated naive and preexposed mice (**Figure 5I**), and a similar capacity to produce IFNγ upon non-specific stimulation with PMA/ionomycin or upon specific stimulation with Reo-infected target cells (**Figure 5J**). Additionally, their recognition of Reo-infected target cells was not impaired when NAb-containing plasma from preexposed mice was added to the system. Altogether, these data demonstrate that the intratumoral presence of functional T cells is not affected by preexposure to Reo.

Combined Reo and T-cell-based immunotherapy retains its efficacy in preexposed mice

Since the total Reo-induced influx and activation of $CD8^+$ T cells was not impaired in preexposed mice, we expected that the combination of Reo and T-cell-based immunotherapy would still be effective in this setting. We first investigated the efficacy of Reo&CD3-bsAb therapy in the KPC3.TRP1 tumor model (**Figure 6A**). As demonstrated before, preexposure induced high levels of NAbs (**Figure 6B**) and the presence of Reo-specific T cells (**Figure 6C**) in the circulation. We treated both naive and preexposed mice bearing KPC3.TRP1 tumors with Reo&CD3-bsAb therapy and observed that tumors of all Reo&CD3-bsAb-treated mice regressed in volume, irrespective of their preexposure status (**Figure 6D**). Although the survival time after Reo&CD3-bsAbs therapy was decreased in preexposed mice compared to naive mice (**Figure 6E**), these data demonstrate that Reo&CD3-bsAb therapy is still effective in a preexisting immunity setting.

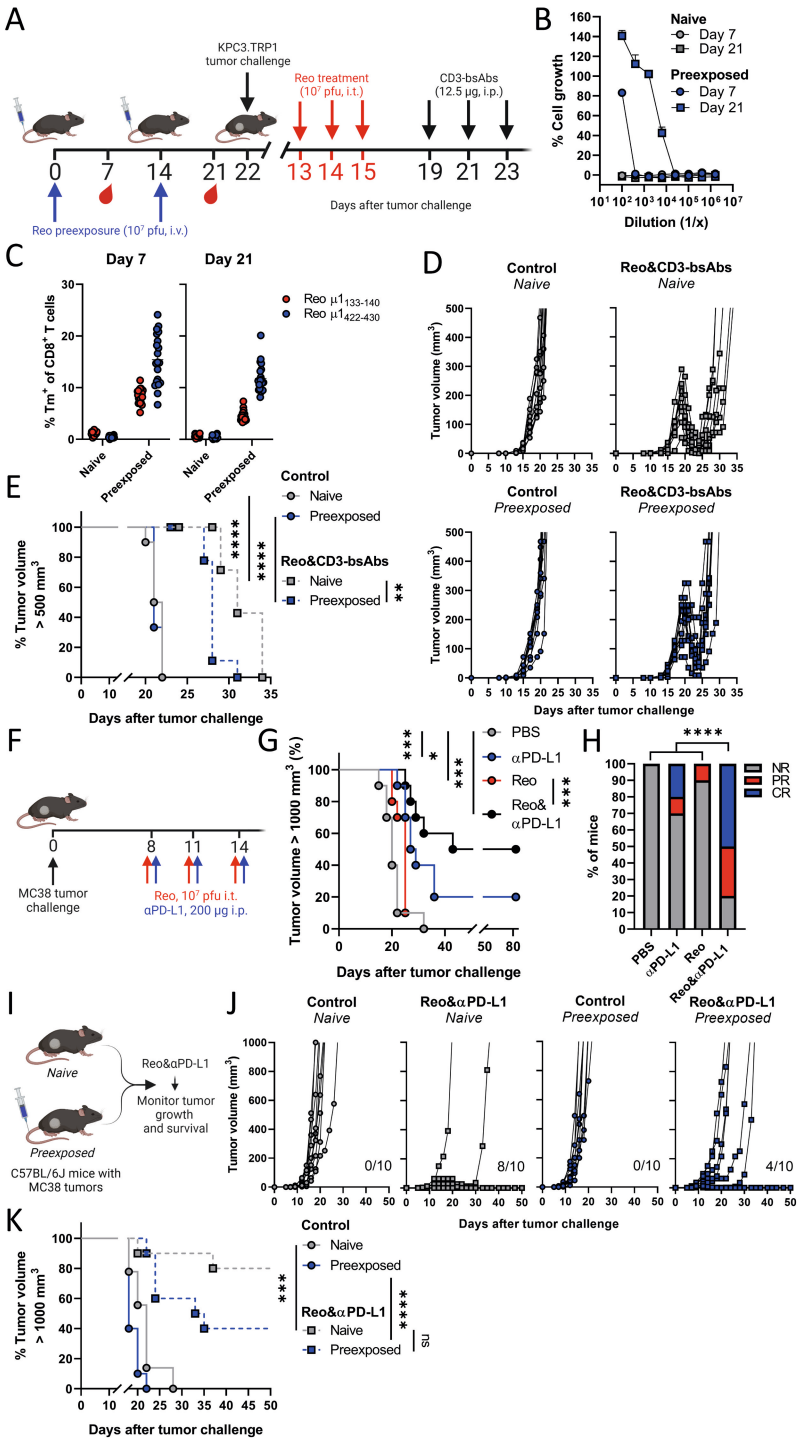


Figure 6. Combined Reo and T-cell-based immunotherapy retains its efficacy in preexposed mice. (**A**) Overview of experiment described in (B-E). Male C57BL/6J mice (n=10/group) were preexposed by intravenous (i.v.) injection of Reo (10^7 plaque-forming units (pfu)/injection) on days 0 and 14. After preexposure, mice were subcutaneously inoculated with KPC3.TRP1 cells >>

>> (1x10^5/mouse) and received intratumoral (i.t.) Reo injections (10^7 pfu/injection) on indicated days, followed by intraperitoneal (i.p.) administration of CD3-bsAbs (12.5 µg/injection). (**B**) Reo neutralization assay. Average dilution curves using plasma harvested on indicated days. (**C**) Reo-specific $\mu1_{133-140}$ and $\mu1_{422-430}$ tetramer (Tm)$^+$ $CD8^+$ T cells in the circulation on indicated days. (**D**) Individual growth curves of naive or preexposed mice receiving Reo&CD3-bsAb therapy. (**E**) Kaplan-Meier survival graphs of mice after indicated treatments. (**F**) Overview of experiment described in (G, H). Male C57BL/6J mice (n=10/group) were subcutaneously engrafted with MC38 cells (5x10^5/mouse) and received Reo (i.t., 10^7 pfu/injection) and αPD-L1 (i.p., 200 µg/injection) on day 8, 11 and 14. (**G**) Kaplan-Meier survival graphs of mice after indicated treatments. (**H**) Frequency of Non-Responders (NR), Partial Responders (PR), or Complete Responders (CR) within each treatment group. (**I**) Overview of experiment described in (J, K). Male C57BL/6J mice (n=10/group) were preexposed as described in (A). After preexposure, mice were subcutaneously inoculated with MC38 cells (5x10^5/mouse) and received Reo&αPD-L1 therapy as described in (F). (**J**) Individual growth curves of naive or preexposed mice receiving Reo&αPD-L1 therapy. Indicated is the number of tumor-free mice in each experimental group. (**K**) Kaplan-Meier survival graphs of mice after indicated treatments. Data represent mean±SEM. Log-rank tests were used to compare differences in survival in (E), (G), and (K). Chi-square test was used to determine statistical differences in response in (H). Significance levels: ns=not significant, *p<0.05, **p<0.01, ***p<0.001, and ****p<0.0001.

To assess the role of Reo preexisting immunity in a different combinatorial immunotherapeutic strategy, we employed the chemically-induced preclinical colon model MC38, which shows a partial response to checkpoint blockade therapy (αPD-L1) (37). We first assessed whether Reo was able to enhance the efficacy of αPD-L1. Reo was administered intratumorally on days 8, 11, and 14 after tumor challenge, and αPD-L1 therapy was applied intraperitoneally on the same days (**Figure 6F**). While αPD-L1 alone delayed tumor growth and induced complete tumor clearance in 20% of animals, Reo&αPD-L1 therapy led to tumor clearance in 50% of animals (**Figure 6G, H**). We concluded that the combination of Reo&αPD-L1 is very effective in the MC38 tumor model, and subsequently investigated the impact of preexposure to Reo on its efficacy (**Figure 6I**). Similar to what was observed for Reo&CD3-bsAbs, preexposure to Reo (**Figure S9A, B**) did influence the efficacy of Reo&αPD-L1 therapy, but complete tumor clearance could still be observed in 40% of preexposed mice (**Figure 6J, K**). These data indicate that Reo preexposure does not preclude the use of Reo and T-cell-based combination therapy for effective tumor control.

Reo-based combination therapy remains effective upon repeated systemic administration

Given that preexposure does not hamper the efficacy of Reo-based combination therapies when Reo is administered intratumorally, we finally investigated the efficacy of Reo-based combination therapy in a more clinically-relevant setting. In the clinic, intravenous administration is preferred over intratumoral administration, since it limits patients' discomfort and allows for the simultaneous targeting of multiple tumor lesions, irrespective of their location. In addition, patients are preferably treated with repeated infusions, which will result in multiple boosting events of Reo-directed immunity that might impair therapeutic efficacy. We therefore investigated the consequences of repeated intravenous (i.v.) Reo infusions on Reo infection and the Reo-induced influx of immune cells (**Figure 7A**). For this experiment, the clinical-grade formulation of Reo, named Pelareorep (Pela in graphs) was used. Indeed, repeated i.v. Pelareorep injections

impaired the presence of virus in tumors (**Figure 7B**). While Reo S4 genomic copies could be found in tumors of mice that received only 1 injection with Pelareorep, this greatly diminished after multiple infusions. A similar pattern was observed with the expression of ISGs (**Figure 7C**). Importantly, while the frequency of NK cells decreased after the first infusion (**Figure 7D**), the frequency of intratumoral CD8$^+$ T cells remained constant over time after repeated i.v. Pelareorep injections (**Figure 7E**). We next investigated whether the combination therapy of i.v. administered Pelareorep combined with CD3-bsAbs would still be effective. We compared the efficacy of i.v. Pelareorep&CD3-bsAb administered as multiple cycles with a 5-day interval, with our previously defined regimen which comprises 1 cycle of 3 consecutive virus infusions followed by CD3-bsAb administrations (**Figure 7F**) (3). Both regimens were equally effective (**Figure 7G, H**), demonstrating that systemic and repeated Reo administration is not a barrier to the antitumor efficacy of combined Reo and T-cell-based immunotherapy. Altogether, these data demonstrate that the use of Reo as an oncolytic agent is hampered by the presence of NAbs, but T cells are still attracted towards the tumor and combined Reo and T-cell-based immunotherapy remained effective.

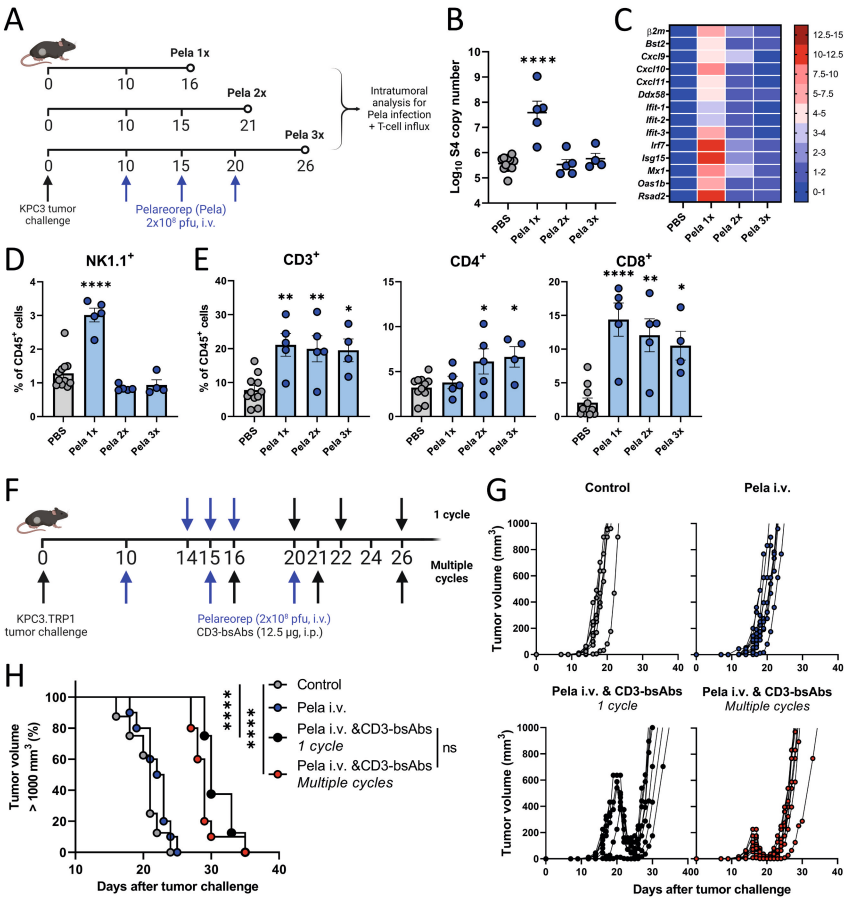


Figure 7. Reo-based combination therapy remains effective upon repeated systemic administration. (**A**) Overview of experiment described in (B-E). Male C57BL/6J mice (n=5/group) >>

>> were subcutaneously inoculated with KPC3 cells (1x10^5/mouse) and intravenously (i.v.) injected with Pelareorep (Pela; 2x10^8 plaque-forming units (pfu)/injection) on indicated days. Mice were sacrificed after 1, 2, or 3 Pela infusions for intratumoral analysis. (**B**) Intratumoral presence of genomic copies of Reo S4 segment, as measured by quantitative reverse transcription PCR (RT-qPCR). (**C**) Heatmap depicting relative expression of various interferon response genes in tumors harvested after 1, 2, or 3 Pela infusions, as determined by RT-qPCR. (**D**) Intratumoral frequency of NK cells within CD45$^+$ immune cells. (**E**) Intratumoral frequency of CD3$^+$, CD4$^+$, and CD8$^+$ T cells within CD45$^+$ immune cells. (**F**) Overview of experiment described in (G, H). Male C57BL/6J mice (n=8-10/group) were subcutaneously inoculated with KPC3.TRP1 cells (1x10^5/mouse) and received i.v. injections with Pela (2x10^8 pfu/injection) and intraperitoneal (i.p.) injections with CD3-bsAbs (12.5 **μ**g/injection) on indicated days. (**G**) Individual tumor growth curves of mice receiving indicated treatments. (**H**) Kaplan-Meier survival graphs of mice after indicated treatments. Data represent mean±SEM. Differences between groups in (B), (D), and (E) against the PBS-treated group was determined using an ordinary one-way analysis of variance (ANOVA) with Dunnett's post hoc test. Log-rank tests were used to compare differences in survival in (H). Significance levels: ns=not significant, *p<0.05, **p<0.01, and ****p<0.0001.

DISCUSSION

Here, we tackled an important topic of debate in the field of oncolytic virus (OV) therapy, by investigating the impact of preexisting immunity, in particular the role of neutralizing antibodies (NAbs), on the antitumor efficacy of oncolytic Reovirus (Reo). Our data demonstrated that preexposure-induced Reo-specific NAbs are detrimental to Reo infection and Reo-induced tumor control when used as monotherapy. In contrast, the Reo-induced influx of T cells was not affected by NAbs and Reo-based combinatorial immunotherapy remained effective in preexposed mice.

It currently remains unknown why the Reo-induced T-cell influx remained unaffected by preexposure, even though the copy numbers of Reo and the expression of ISGs in tumors were impaired. However, a similar observation was made in a study where immunocompetent naive or Newcastle disease virus (NDV)-exposed B16.F10-bearing C57BL/6J mice were intratumorally injected with NDV (38). Although viral replication was decreased in preexposed mice, the NDV-induced intratumoral influx of CD8$^+$ T cells was comparable between naive and preexposed animals. In our studies, it might be possible that the remaining moderate expression of T-cell-attracting chemokine *Cxcl9* in tumors of preexposed mice was sufficient to attract T cells to the tumor. In contrast to *Cxcl10* and *Cxcl11* which are induced by both type I and type II IFN, *Cxcl9* is only induced by type II IFN, which might contribute to this different expression pattern (39). Furthermore, the expression of ISGs was strongly reduced in the presence of NAbs, but not completely abrogated. Since interferons are powerful immune mediators, a very moderate IFN response, either induced by Reo itself, incoming T cells or NK cells, or by the transmission of an antiviral state from a few Reo-infected tumor cells to neighboring tumor cells, might have been sufficient to induce T-cell attraction to the tumor (40,41).

Alternatively, it is possible that administration of Reo to preexposed mice did not completely preclude effective viral infection and ISG expression, but that the presence

of Reo, the expression of ISGs, and the subsequent influx of T cells might follow different kinetics in preexposed mice compared to naive mice. The preexisting NAbs will presumably lead to faster clearance of the virus, even upon intratumoral injection. However, a short presence of Reo in the tumor might already have been sufficient to attract and maintain T cells in the tumor, without the need for continued viral presence.

Lastly, the processing and presentation of viral epitopes are expected to be affected by the presence of NAbs (42), which might also explain why a different Reo-specific $CD8^+$ T-cell population is dominant in tumors of preexposed mice. Although the presence of Reo itself is diminished, this does not directly preclude the presentation of viral epitopes. A continued presentation of viral epitopes might thus retain $CD8^+$ T cells in the tumor. While these observations provide interesting avenues for further research, we concluded here that the impaired Reo infection observed in preexposed mice, or upon repeated intravenous Reo infusions, does not preclude effective intratumoral T-cell influx and thus permits potent antitumor responses upon combinatorial Reo and T-cell-based immunotherapy.

The conclusion that NAbs present a barrier to the antitumor efficacy of Reo monotherapy may be surprising, since previous studies suggested that NAbs are beneficial (14,15). However, the beneficial role of NAbs has only been demonstrated in the context of immune cell carriage. For instance, mechanistic studies have shown that Reo can be taken up and internalized by various immune cells, including human monocytes, DCs, and T cells (13-15,43,44). Here, the presence of NAbs can contribute to enhanced uptake, since Reo/NAb complexes are more efficiently internalized by immune cells compared to Reo particles alone. Thus, NAbs might be beneficial specifically when employing cellular carriers for Reo delivery to tumors, but the effect of NAbs on the antitumor efficacy of Reo remained unknown. Here, we unequivocally demonstrate that the presence of NAbs restricts the antitumor efficacy of Reo therapy, even when administered intratumorally.

Since a large proportion of the human population, including cancer patients, has been preexposed to Reo and thus has circulating NAbs, our data may explain why Reo monotherapy has not yet reached optimal efficacy in prior clinical studies. Still, various approaches, including the above-mentioned use of immune cell carriage, have been proposed to enhance the delivery of Reo particles to tumors in the presence of NAbs (7). For instance, the use of a low dosage of the chemotherapeutic drug cyclophosphamide (CPA) leads to the depletion of regulatory T cells and enhanced tumor-specific $CD8^+$ T-cell responses (45,46), but can also ablate the production of NAbs, leading to enhanced anticancer efficacy of Reo therapy (47,48). Although these preclinical results were encouraging, compiled data from various Phase I clinical trials demonstrated that the effect of CPA or other chemotherapeutic drugs such as gemcitabine and docetaxel only moderately reduced Reo-specific NAb responses (49). Additionally, the use of CPA or other chemotherapeutics to prevent NAb production

might only be relevant for individuals that have not been exposed to Reo before, which is a minority of patients. Alternatively, it might be possible to employ certain apheresis techniques such as plasma exchange (50) or immunoadsorption (51) in seropositive patients, which are already applied in the context of autoimmune diseases and organ transplants. Especially immunoadsorption ensures rapid removal of specific antibodies from the circulation, and might be performed in seropositive patients before Reo therapy to greatly reduce the level of preexisting NAbs. However, the activation of Reo-specific B cells upon the first therapeutic Reo administration will lead to rapidly emerging new NAbs that will hamper the efficacy of subsequent infusions.

The above-mentioned strategies could be employed to reduce, circumvent, or remove NAb responses to increase the efficacy of Reo monotherapy. However, our data strongly suggest that these efforts might not be necessary. We expect that combined Reo and checkpoint blockade, which has already demonstrated potent responses in various preclinical models (52,53), and is currently the subject of various clinical trials, as well as other combinatorial strategies that also rely on the effective Reo-induced influx of T cells, such as T-cell-engagers (3), vaccination (30) or the use of dual-specific CAR T cells (54) should be able to demonstrate potent antitumor responses in the presence of NAbs. Thus, our data are encouraging for ongoing and future clinical trials investigating the efficacy of Reo and T-cell-based immunotherapeutic strategies, even in the context of intravenous Reo administration.

Altogether, given the high prevalence of seropositivity for Reo in cancer patients, this study strongly advocates for the use of Reo as part of a T-cell-based combinatorial approach to unleash its full potential and allow maximal anticancer efficacy, without obstruction by preexisting immune responses.

DECLARATIONS

Acknowledgments. The authors gratefully acknowledge the operators of the Flow Cytometry Core Facility (FCF) of the LUMC and the Animal Facility of the LUMC for their excellent support and care of the animals, respectively. The hybridoma 10F6 (reovirus μ1), developed by T. S. Dermody from the University of Pittsburgh School of Medicine, was obtained from the Developmental Studies Hybridoma Bank, created by the NICHD of the NIH and maintained at The University of Iowa, Department of Biology, Iowa City, IA 52242. All figures regarding experimental designs are created with BioRender.com.
Author contributions. Conceptualization: CG, TvH, NvM. Methodology: CG, PK, LG, CL, DvdW, RH, TvH, NvM. Formal analysis: CG. Investigation: CG, PK, OR. Resources: DvdW, RH, MC, LH, EMEV, MJPW. Writing – Original Draft: CG, NvM. Writing - Review & Editing: CG, SHvdB, TvH, NvM. Visualization: CG. Supervision: NvM. Funding acquisition: TvH, NvM. All authors approved the final version of the manuscript.

Funding. This work was financially supported by a PhD fellowship from Leiden University Medical Center (to CG), a research grant from Oncolytics Biotech Inc. (to TvH and NvM) and the Support Casper campaign by the Dutch foundation 'Stichting Overleven met Alvleesklierkanker' (supportcasper.nl) project number SOAK 22.02 (to NvM).

Competing interests. MC and HL are employees of Oncolytics Biotech Inc. TvH and NvM received funding from Oncolytics Biotech Inc. in the past. All other authors declare no conflict of interest. The funders had no role in the design of the study; in the collection, analyses, or interpretation of data; in the writing of the manuscript, or in the decision to publish the results.

Data availability statement. All data relevant to this study are included in the main text or the supplementary materials and are available on reasonable request.

REFERENCES

1. Groeneveldt C, van Hall T, van der Burg SH, Ten Dijke P, van Montfoort N. Immunotherapeutic Potential of TGF-β Inhibition and Oncolytic Viruses. Trends Immunol **2020**;41:406-20
2. Müller L, Berkeley R, Barr T, Ilett E, Errington-Mais F. Past, Present and Future of Oncolytic Reovirus. Cancers (Basel) **2020**;12
3. Groeneveldt C, Kinderman P, van den Wollenberg DJM, van den Oever RL, Middelburg J, Mustafa DAM*, et al.* Preconditioning of the tumor microenvironment with oncolytic reovirus converts CD3-bispecific antibody treatment into effective immunotherapy. J Immunother Cancer **2020**;8:e001191
4. Morris DG, Feng X, DiFrancesco LM, Fonseca K, Forsyth PA, Paterson AH*, et al.* REO-001: A phase I trial of percutaneous intralesional administration of reovirus type 3 dearing (Reolysin®) in patients with advanced solid tumors. Investigational new drugs **2013**;31:696-706
5. Vidal L, Pandha HS, Yap TA, White CL, Twigger K, Vile RG*, et al.* A Phase I Study of Intravenous Oncolytic Reovirus Type 3 Dearing in Patients with Advanced Cancer. Clinical Cancer Research **2008**;14:7127-37
6. Forsyth P, Roldán G, George D, Wallace C, Palmer CA, Morris D*, et al.* A Phase I Trial of Intratumoral Administration of Reovirus in Patients With Histologically Confirmed Recurrent Malignant Gliomas. Molecular Therapy **2008**;16:627-32
7. Groeneveldt C, van den Ende J, van Montfoort N. Preexisting immunity: Barrier or bridge to effective oncolytic virus therapy? Cytokine & Growth Factor Reviews **2023**;70:1-12
8. Tai JH, Williams JV, Edwards KM, Wright PF, Crowe JJE, Dermody TS. Prevalence of Reovirus-Specific Antibodies in Young Children in Nashville, Tennessee. J Infect Disease **2005**;191:1221-4
9. White CL, Twigger KR, Vidal L, De Bono JS, Coffey M, Heinemann L*, et al.* Characterization of the adaptive and innate immune response to intravenous oncolytic reovirus (Dearing type 3) during a phase I clinical trial. Gene Therapy **2008**;15:911-20
10. Lolkema MP, Arkenau H-T, Harrington K, Roxburgh P, Morrison R, Roulstone V*, et al.* A Phase I Study of the Combination of Intravenous Reovirus Type 3 Dearing and Gemcitabine in Patients with Advanced Cancer. Clinical Cancer Research **2011**;17:581-8
11. Comins C, Spicer J, Protheroe A, Roulstone V, Twigger K, White CM*, et al.* REO-10: A Phase I Study of Intravenous Reovirus and Docetaxel in Patients with Advanced Cancer. Clinical Cancer Research **2010**;16:5564-72
12. Galanis E, Markovic SN, Suman VJ, Nuovo GJ, Vile RG, Kottke TJ*, et al.* Phase II trial of intravenous administration of Reolysin(®) (Reovirus Serotype-3-dearing Strain) in patients with metastatic melanoma. Mol Ther **2012**;20:1998-2003
13. Adair RA, Roulstone V, Scott KJ, Morgan R, Nuovo GJ, Fuller M*, et al.* Cell Carriage, Delivery, and Selective Replication of an Oncolytic Virus in Tumor in Patients. Science Translational Medicine **2012**;4
14. Berkeley RA, Steele LP, Mulder AA, van den Wollenberg DJM, Kottke TJ, Thompson J*, et al.* Antibody-Neutralized Reovirus Is Effective in Oncolytic Virotherapy. Cancer Imm Res **2018**;6:1161-73
15. Ilett E, Kottke T, Donnelly O, Thompson J, Willmon C, Diaz R*, et al.* Cytokine Conditioning Enhances Systemic Delivery and Therapy of an Oncolytic Virus. Molecular Therapy **2014**;22:1851-63
16. Dijkgraaf EM, Santegoets SJ, Reyners AK, Goedemans R, Wouters MC, Kenter GG*, et al.* A phase I trial combining carboplatin/doxorubicin with tocilizumab, an anti-IL-6R monoclonal antibody, and interferon-α2b in patients with recurrent epithelial ovarian cancer. Annals of oncology : official journal of the European Society for Medical Oncology **2015**;26:2141-9
17. Verdegaal E, van der Kooij MK, Visser M, van der Minne C, de Bruin L, Meij P*, et al.* Low-dose interferon-alpha preconditioning and adoptive cell therapy in patients with metastatic melanoma refractory to standard (immune) therapies: a phase I/II study. J Immunother Cancer **2020**;8

18. Santegoets SJ, van Ham VJ, Ehsan I, Charoentong P, Duurland CL, van Unen V*, et al.* The Anatomical Location Shapes the Immune Infiltrate in Tumors of Same Etiology and Affects Survival. Clin Cancer Res **2019**;25:240-52
19. Speetjens FM, Kuppen PJ, Welters MJ, Essahsah F, Voet van den Brink AM, Lantrua MG*, et al.* Induction of p53-specific immunity by a p53 synthetic long peptide vaccine in patients treated for metastatic colorectal cancer. Clin Cancer Res **2009**;15:1086-95
20. van den Wollenberg DJM, Dautzenberg IJC, van den Hengel SK, Cramer SJ, de Groot RJ, Hoeben RC. Isolation of reovirus T3D mutants capable of infecting human tumor cells independent of junction adhesion molecule-A. PLoS One **2012**;7:e48064-e
21. Smith RE, Zweerink HJ, Joklik WK. Polypeptide components of virions, top component and cores of reovirus type 3. Virology **1969**;39:791-810
22. Fallaux FJ, Kranenburg O, Cramer SJ, Houweling A, Van Ormondt H, Hoeben RC*, et al.* Characterization of 911: a new helper cell line for the titration and propagation of early region 1-deleted adenoviral vectors. Human gene therapy **1996**;7:215-22
23. Hingorani SR, Wang L, Multani AS, Combs C, Deramaudt TB, Hruban RH*, et al.* Trp53R172H and KrasG12D cooperate to promote chromosomal instability and widely metastatic pancreatic ductal adenocarcinoma in mice. Cancer cell **2005**;7:469-83
24. Benonisson H, Altıntaş I, Sluijter M, Verploegen S, Labrijn AF, Schuurhuis DH*, et al.* CD3-Bispecific Antibody Therapy Turns Solid Tumors into Inflammatory Sites but Does Not Install Protective Memory. Molecular cancer therapeutics **2019**;18:312-22
25. Lin K-Y, Guarnieri FG, Staveley-O'Carroll KF, Levitsky HI, August JT, Pardoll DM*, et al.* Treatment of Established Tumors with a Novel Vaccine That Enhances Major Histocompatibility Class II Presentation of Tumor Antigen. Cancer Res **1996**;56:21-6
26. Belkina AC, Ciccolella CO, Anno R, Halpert R, Spidlen J, Snyder-Cappione JE. Automated optimized parameters for T-distributed stochastic neighbor embedding improve visualization and analysis of large datasets. Nature Communications **2019**;10:5415
27. Murphy JP, Kim Y, Clements DR, Konda P, Schuster H, Kowalewski DJ*, et al.* Therapy-Induced MHC I Ligands Shape Neo-Antitumor CD8 T Cell Responses during Oncolytic Virus-Based Cancer Immunotherapy. J Proteome Res **2019**;18:2666-75
28. Mijatovic-Rustempasic S, Tam KI, Kerin TK, Lewis JM, Gautam R, Quaye O*, et al.* Sensitive and specific quantitative detection of rotavirus A by one-step real-time reverse transcription-PCR assay without antecedent double-stranded-RNA denaturation. Journal of clinical microbiology **2013**;51:3047-54
29. Dupont WD, Plummer WD, Jr. Power and sample size calculations. A review and computer program. Controlled clinical trials **1990**;11:116-28
30. Groeneveldt C, Kinderman P, van Stigt Thans JJC, Labrie C, Griffioen L, Sluijter M*, et al.* Preinduced reovirus-specific T-cell immunity enhances the anticancer efficacy of reovirus therapy. Journal for ImmunoTherapy of Cancer **2022**;10:e004464
31. Loken SD, Norman K, Hirasawa K, Nodwell M, Lester WM, Demetrick DJ. Morbidity in immunosuppressed (SCID/NOD) mice treated with reovirus (Dearing 3) as an anti-cancer biotherapeutic. Cancer Biology & Therapy **2004**;3:734-8
32. Kim M, Garant KA, zur Nieden NI, Alain T, Loken SD, Urbanski SJ*, et al.* Attenuated reovirus displays oncolysis with reduced host toxicity. Br J Cancer **2011**;104:290-9
33. Dina Zita M, Phillips MB, Stuart JD, Kumarapeli AR, Snyder AJ, Paredes A*, et al.* The M2 Gene Is a Determinant of Reovirus-Induced Myocarditis. J Virol **2022**;96:e0187921
34. Samson A, Scott KJ, Taggart D, West EJ, Wilson E, Nuovo GJ*, et al.* Intravenous delivery of oncolytic reovirus to brain tumor patients immunologically primes for subsequent checkpoint blockade. Sci Transl Med **2018**;10:eaam7577
35. Collienne M, Loghmani H, Heineman TC, Arnold D. GOBLET: a phase I/II study of pelareorep and atezolizumab +/- chemo in advanced or metastatic gastrointestinal cancers. Future oncology (London, England) **2022**;18:2871-8

36. Sivanandam V, LaRocca CJ, Chen NG, Fong Y, Warner SG. Oncolytic Viruses and Immune Checkpoint Inhibition: The Best of Both Worlds. Molecular Therapy - Oncolytics **2019**;13:93-106
37. Kleinovink JW, Marijt KA, Schoonderwoerd MJA, van Hall T, Ossendorp F, Fransen MF. PD-L1 expression on malignant cells is no prerequisite for checkpoint therapy. Oncoimmunology **2017**;6:e1294299
38. Ricca JM, Oseledchyk A, Walther T, Liu C, Mangarin L, Merghoub T*, et al.* Pre-existing Immunity to Oncolytic Virus Potentiates Its Immunotherapeutic Efficacy. Molecular Therapy **2018**;26:1008-19
39. Tokunaga R, Zhang W, Naseem M, Puccini A, Berger MD, Soni S*, et al.* CXCL9, CXCL10, CXCL11/CXCR3 axis for immune activation - A target for novel cancer therapy. Cancer treatment reviews **2018**;63:40-7
40. Vitiello GAF, Ferreira WAS, Cordeiro de Lima VC, Medina TDS. Antiviral Responses in Cancer: Boosting Antitumor Immunity Through Activation of Interferon Pathway in the Tumor Microenvironment. Front Immunol **2021**;12:782852
41. Geoffroy K, Bourgeois-Daigneault M-C. The pros and cons of interferons for oncolytic virotherapy. Cytokine & Growth Factor Reviews **2020**;56:49-58
42. van Montfoort N, Mangsbo SM, Camps MGM, van Maren WWC, Verhaart IEC, Waisman A*, et al.* Circulating specific antibodies enhance systemic cross-priming by delivery of complexed antigen to dendritic cells in vivo. European Journal of Immunology **2012**;42:598-606
43. Ilett EJ, Bárcena M, Errington-Mais F, Griffin S, Harrington KJ, Pandha HS*, et al.* Internalization of Oncolytic Reovirus by Human Dendritic Cell Carriers Protects the Virus from Neutralization. Clinical Cancer Research **2011**;17:2767-76
44. Roulstone V, Khan K, Pandha HS, Rudman S, Coffey M, Gill GM*, et al.* Phase I trial of cyclophosphamide as an immune modulator for optimizing oncolytic reovirus delivery to solid tumors. Clin Cancer Res **2015**;21:1305-12
45. Ghiringhelli F, Menard C, Puig PE, Ladoire S, Roux S, Martin F*, et al.* Metronomic cyclophosphamide regimen selectively depletes CD4+CD25+ regulatory T cells and restores T and NK effector functions in end stage cancer patients. Cancer Immunol Immunother **2007**;56:641-8
46. Scurr M, Pembroke T, Bloom A, Roberts D, Thomson A, Smart K*, et al.* Low-Dose Cyclophosphamide Induces Antitumor T-Cell Responses, which Associate with Survival in Metastatic Colorectal Cancer. Clin Cancer Res **2017**;23:6771-80
47. Qiao J, Wang H, Kottke T, White C, Twigger K, Diaz RM*, et al.* Cyclophosphamide Facilitates Antitumor Efficacy against Subcutaneous Tumors following Intravenous Delivery of Reovirus. Clinical Cancer Research **2008**;14:259-69
48. Kottke T, Thompson J, Diaz RM, Pulido J, Willmon C, Coffey M*, et al.* Improved Systemic Delivery of Oncolytic Reovirus to Established Tumors Using Preconditioning with Cyclophosphamide-Mediated Treg Modulation and Interleukin-2. Clinical Cancer Research **2009**;15:561-9
49. Roulstone V, Mansfield D, Harris RJ, Twigger K, White C, de Bono J*, et al.* Antiviral antibody responses to systemic administration of an oncolytic RNA virus: the impact of standard concomitant anticancer chemotherapies. Journal for ImmunoTherapy of Cancer **2021**;9:e002673-e
50. Weinstein R. Basic principles of therapeutic plasma exchange. Transfusion and Apheresis Science **2023**;62:103675
51. Braun N, Bosch T. Immunoadsorption, current status and future developments. Expert opinion on investigational drugs **2000**;9:2017-38
52. Mostafa AA, Meyers DE, Thirukkumaran CM, Liu PJ, Gratton K, Spurrell J*, et al.* Oncolytic Reovirus and Immune Checkpoint Inhibition as a Novel Immunotherapeutic Strategy for Breast Cancer. Cancers **2018**;10

53. Augustine T, John P, Friedman T, Jiffry J, Guzik H, Mannan R*, et al.* Potentiating effect of reovirus on immune checkpoint inhibition in microsatellite stable colorectal cancer. Front Oncol **2022**;12
54. Evgin L, Kottke T, Tonne J, Thompson J, Huff AL, van Vloten J*, et al.* Oncolytic virus-mediated expansion of dual-specific CAR T cells improves efficacy against solid tumors in mice. Sci Transl Med **2022**;14:eabn2231

SUPPLEMENTARY FIGURES

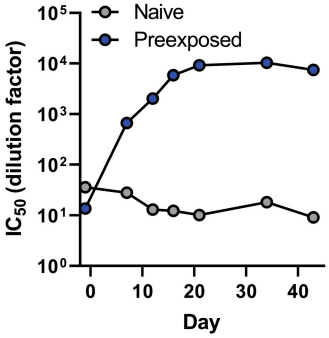


Figure S1. Kinetics of neutralizing antibodies after preexposure. Graph depicts IC_{50} values of pooled plasma (n=6 mice/group) of indicated groups that were harvested on indicated days and subjected to a Reo neutralization assay. IC_{50} values were calculated using non-linear regression analysis.

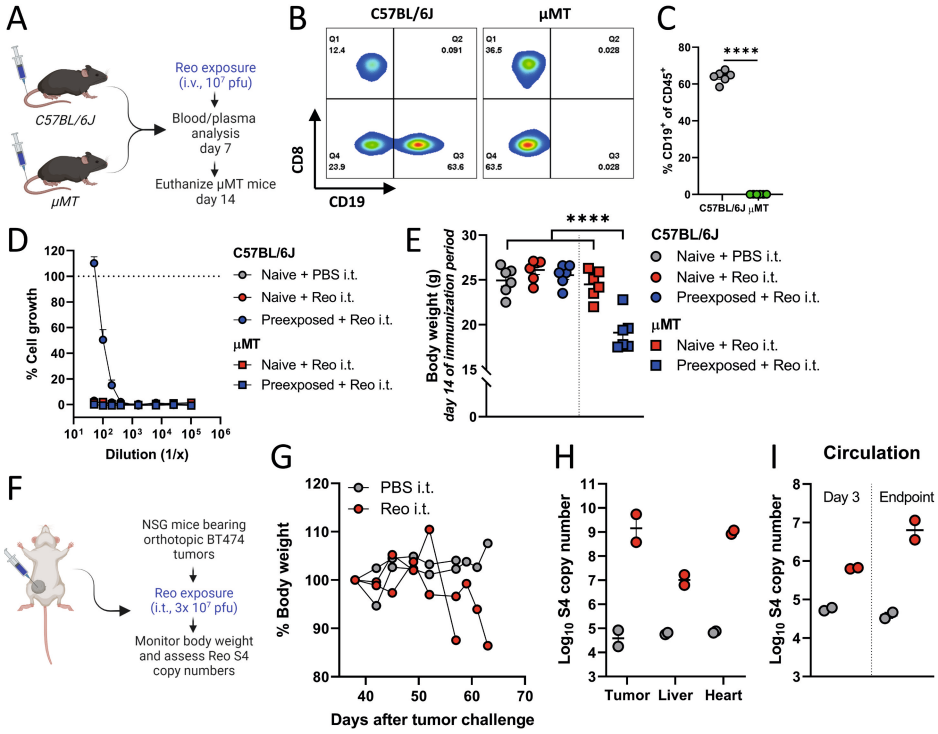


Figure S2. Neutralizing antibodies are required to prevent Reo-induced weight loss and viremia. (**A**) Overview of experiment described in (B-E). Male C57BL/6J or µMT mice (n=6/group) were exposed to Reo by intravenous (i.v.) injection (10^7 plaque-forming units (pfu)/injection) on day 0. (**B**) Representative flow cytometry plots of $CD19^+$ B cells in the circulation of C57BL/6J or µMT mice. (**C**) Quantification of $CD19^+$ B cells in the circulation. (**D**) Reo neutralization assay. Average dilution curves using plasma from indicated groups, harvested on day 7 after preexposure. (**E**) Body weight on day 14 after Reo exposure.

>>

>> (**F**) NSG mice (n=2/group) were inoculated orthotopically with BT474 tumor cells (5x10^6/mouse) in the mammary fat pad and received intratumoral Reo injections (10^7 plaque-forming units (pfu)/injection) on days 37-39. (**G**) Individual changes in body weight during the experiment from the moment of Reo administration. See next page for continuation of figure legend. (**H**) Presence of genomic copies of Reo S4 segment in the tumor, liver, and heart, as measured by quantitative reverse transcription PCR (RT-qPCR). (**I**) Presence of infectious Reo particles in the circulation, as measured by RT-qPCR. Plasma was obtained on day 3 and at the experimental endpoint, and 5 µL was transferred to a monolayer of KPC3 cells. Samples were harvested after 24 hours and subjected to RT-qPCR analysis. Difference between groups in (C) was determined using an unpaired t test, and an ordinary one-way analysis of variance (ANOVA) with Tukey's post hoc test was used to determine differences between groups in (E) Significance level: ****p<0.0001.

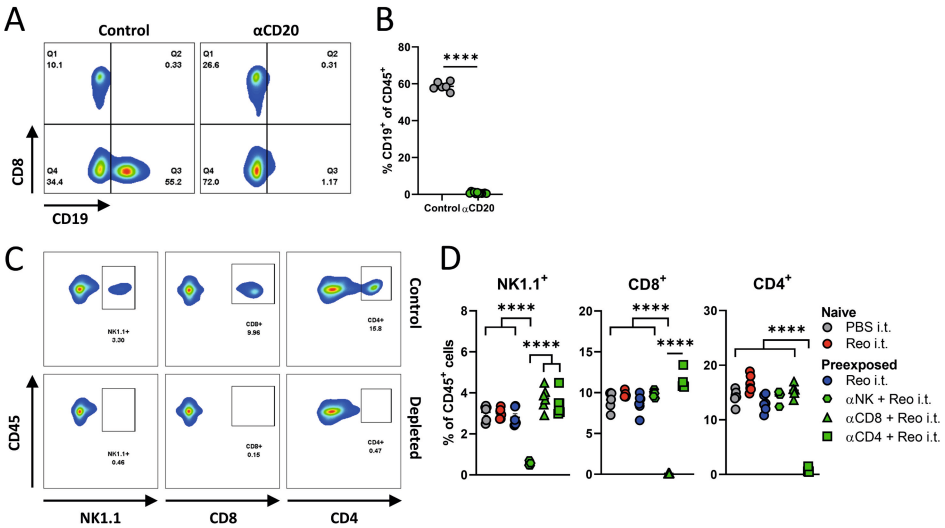


Figure S3. Depletion efficiency during preexposure. (**A**) Representative flow cytometry plots of CD19$^+$ B cells in the circulation after administration of αCD20. (**B**) Quantification of CD19$^+$ B cells in the circulation. (**C**) Representative flow cytometry plots of NK1.1$^+$, CD8$^+$, or CD4$^+$ cells in the circulation after administration of αNK, αCD8, or αCD4 antibodies. (**D**) Quantification of NK1.1$^+$, CD8$^+$, or CD4$^+$ cells in the circulation. Data represent mean±SEM. Differences between groups in (B) were determined using an unpaired t test, and an ordinary one-way analysis of variance (ANOVA) with Tukey's post hoc test was used to determine differences between groups in (D). Significance level: ****p<0.0001.

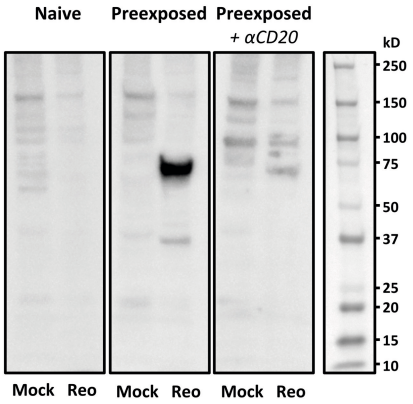


Figure S4. B-cell depletion during preexposure does not completely abrogate the presence of Reo-specific neutralizing antibodies. Western blot of Mock or Reo-infected lysates of HER911 cells using mouse plasma as primary antibody source.

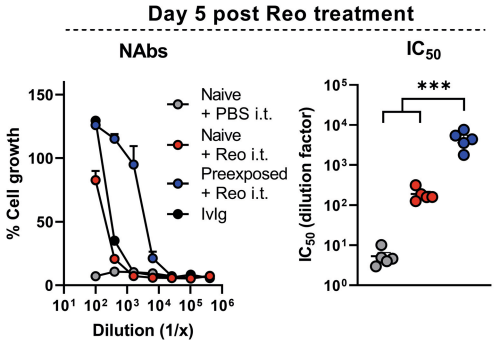


Figure S5. Reo-specific neutralizing antibodies are present 5 days after intratumoral Reo administration. Reo neutralization assay. Average dilution curves using plasma from naive or preexposed mice and individual IC_{50} values on day 5 post intratumoral Reo treatment. Data represent mean±SEM. IC_{50} values were calculated using non-linear regression analysis. Differences between groups were determined using an ordinary one-way analysis of variance (ANOVA) with Tukey's post hoc test. Significance level: ***p<0.001.

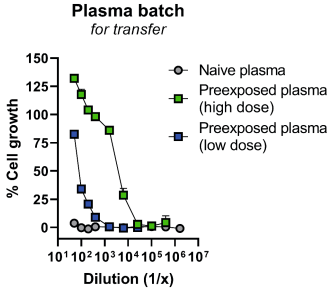


Figure S6. Neutralization capacity of plasma used for the transfer to NSG mice. Reo neutralization assay. Dilution curves were prepared using combined plasma from immunocompetent C57BL/6J naive mice (naive plasma) or C57BL/6J mice that were intravenously preexposed to Reo (preexposed plasma).

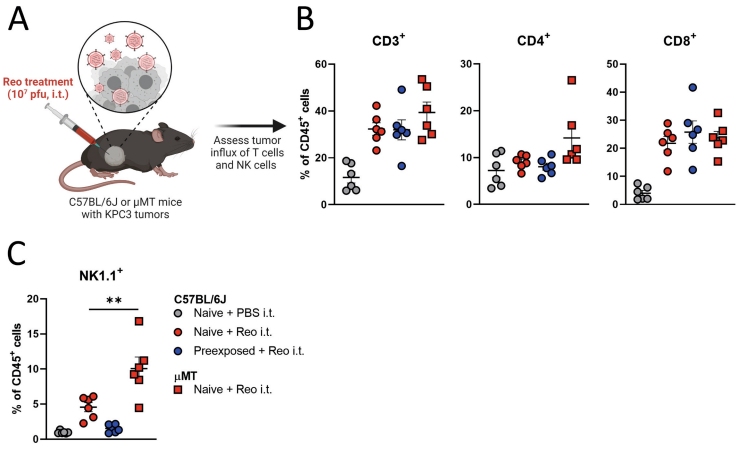


Figure S7. Intratumoral T-cell influx after Reo treatment in µMT or C57BL/6J mice. (**A**) Design of experiment described in (B, C). Male C57BL/6J or µMT mice (n=6/group) were subcutaneously inoculated with KPC3 cells (1x10^5/mouse) and received intratumoral (i.t.) Reo injections (10^7 pfu/injection) on days 13-15. Mice were sacrificed 7 days after Reo administration for ***ex vivo*** analysis. (**B**) Intratumoral frequency of CD3$^+$, CD4$^+$, and CD8$^+$ T cells within CD45$^+$ immune cells. (**C**) Intratumoral frequency of NK cells within CD45$^+$ immune cells. Data represent mean±SEM and differences between groups in (B) and (C) were determined using an ordinary one-way analysis of variance (ANOVA) with Tukey's post hoc test. Significance level: **p<0.01.

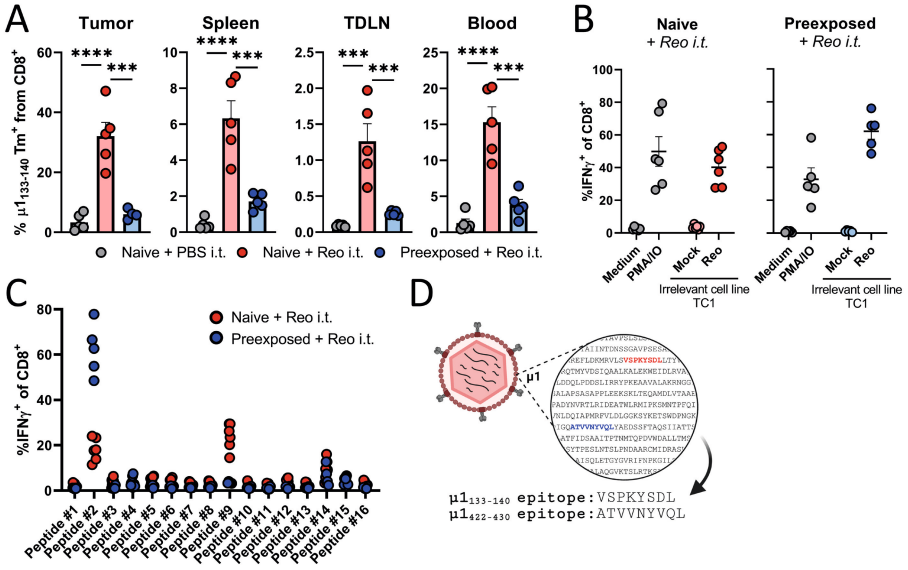


Figure S8. Preexposure affects the specificity of Reo-specific CD8$^+$ T cells. (**A**) Frequency of Reo-specific µ1$_{133-140}$ tetramer (Tm)$^+$ CD8$^+$ T cells in tumor, spleen, tumor-draining lymph node (TDLN), or blood. (**B**) Frequency of interferon gamma (IFNγ)$^+$ cells within the intratumoral CD8$^+$ T-cell population after coculture with indicated targets, as measured with intracellular cytokine staining. PMA/ionomycin (IO) was used as positive control. (**C**) Frequency of IFNγ$^+$ cells within the intratumoral CD8$^+$ T-cell population after coculture with indicated peptides. Each dot represents 1 tumor. (**D**) Schematic overview of sequence and location of both Reo-derived CD8$^+$ T-cell epitopes. Data represent mean±SEM. Differences between groups in (A) were determined using an ordinary one-way analysis of variance (ANOVA) with Tukey's post hoc test. Significance levels: ***p<0.001 and ****p<0.0001.

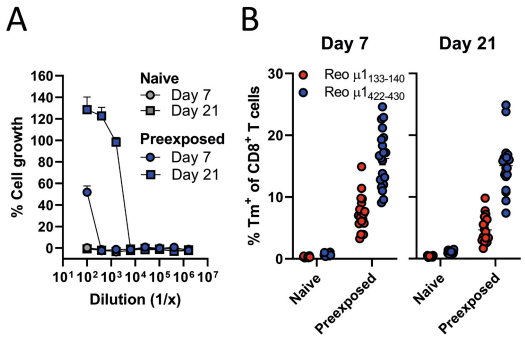


Figure S9. Reo preexposure induces Reo-specific NAbs and CD8⁺ T cells. (**A**) Reo neutralization assay. Average dilution curves using plasma harvested on indicated days. (**B**) Reo-specific $\mu1_{133\text{-}140}$ and $\mu1_{422\text{-}430}$ tetramer $(Tm)^+$ $CD8^+$ T cells in the circulation on indicated days. Data represent mean±SEM.

SUPPLEMENTARY TABLES

Table S1. List of antibodies used for flow cytometric analysis.

	Marker	*Clone*	*Fluorochrome*	*Supplier*
Lymphoid panel	CD45.2	104	FITC	eBioscience
	CD3	145-2C11	PE-CF594	BD Biosciences
	CD8α	53-6.7	Alexa Fluor 700	eBioscience
	Tetramer $\mu1_{133\text{-}140}$		APC	In-house
	Tetramer $\mu1_{422\text{-}430}$		PE	In-house
	CD4	RM4-5	APC	BioLegend
	NK1.1	Pk136	BV650	BD Biosciences
	CD44	IM-7	BV785	BioLegend
	CD62L	MEL-14	BV421	BioLegend
	CD69	H1.2F3	BV605	BioLegend
	KLRG-1	2F1	PE-Cy7	eBioscience
Intracellular cytokine staining panel	CD45.2	104	FITC	eBioscience
	CD3	145-2C11	PE-CF594	BD Biosciences
	CD8α	53-6.7	Alexa Fluor 700	eBioscience
	IFNγ	XMG1.2	APC	BioLegend

Table S2. Sequences of Reo-derived peptides tested using intracellular cytokine staining.

N	*Peptide*	*Allele*	*nM*	*Reo protein*
1	SSVTGIETI	H-2-Db	100.4	λ2
2	ATVVNYVQL	H-2-Db	56.5	μ1
3	HAITNFTKA	H-2-Db	50.1	μ1
4	SALEKTSQI	H-2-Db	1513.6	σ1
5	TGINNANEL	H-2-Db	84.0	λ1
6	HAITNFTKAEM	H-2-Db	46.2	μ1
7	LSTHNGVSL	H-2-Db	1207.8	μ-NS
8	KQLLNTETL	H-2-Db	11.1	λ1
9	VSPKYSDL	H-2-Kb	10.9	μ1
10	FSPGNDFTHM	H-2-Db	137.5	λ3
11	RMNINPTEI	H-2-Db	29.3	λ1
12	NMMVGFETI	H-2-Db	234.4	λ1
13	TRVVNLDQI	H-2-Db	1100.1	μ1
14	AAFLFKTV	H-2-Kb	25.8	σ2
15	INNAFEGRV	H-2-Kb	227.6	σ3
16	YSIMYPTRM	H-2-Kb	83.0	λ1

Table S3. List of primers used for RT-qPCR analysis.

Gene	*Forward*	*Reverse*
S4Q	5′-CGCTTTTGAAGGTCGTGTATCA-3′	5′-CTGGCTGTGCTGAGATTGTTTT-3′
β2M	5′-CTCGGTGACCCTGGTCTTT-3′	5′-CCGTTCTTCAGCATTTGGAT-3′
Bst2	5′-ACATGGCGCCCTCTTTCTATCACT-3′	5′-TGACGGCGAAGTAGATTGTCAGGA-3′
Cxcl9	5′-TGGAGTTCGAGGAACCCTAGT-3′	5′-AGGCAGGTTTGATCTCCGTT-3′
Cxcl10	5′-ACGAACTTAACCACCATCT-3′	5′-TAAACTTTAACTACCCATTGATACATA-3′
Cxcl11	5′-GTTCAAACAGGGGCGCTG-3′	5′-GCATTATGAGGCGAGCTTGC-3′
Ddx58	5′-AAGGCCACAGTTGATCCAAA-3′	5′-TTGGCCAGTTTTCCTTGTCG-3′
Ifit-1	5′-CTGGACAAGGTGGAGAAGGT-3′	5′-AGGGTTTTCTGGCTCCACTT-3′
Ifit-2	5′-TGCTCTTGACTGTGAGGAGG-3′	5′-ATCCAGACGGTAGTTCGCAA-3′
Ifit-3	5′-GTGCAACCAGGTCGAACATT-3′	5′- AGGTGACCAGTCGACGAATT-3′
Irf7	5′-GACCGTGTTTACGAGGAACC-3′	5′-GCTGTACAGGAACACGCATC-3′
Isg15	5′-GGAACGAAAGGGGCCACAGCA-3′	5′-CCTCCATGGGCCTTCCCTCGA-3′
Mx1	5′-GATGGTCCAAACTGCCTTCG-3′	5′-TTGTAAACCTGGTCCTGGCA-3′
Mzt2	5′-TCGGTGCCCATATCTCTGTC-3′	5′-CTGCTTCGGGAGTTGCTTTT-3′
Oas1b	5′-AGCATGAGAGACGTTGTGGA-3′	5′-GCGTAGAATTGTTGGTTAGGCT-3′
Ptp4a2	5′-AGCCCCTGTGGAGATCTCTT-3′	5′-AGCATCACAAACTCGAACCA-3′
Rsad2	5′-GGTGCCTGAATCTAACCAGAAG-3′	5′-CCACGCCAACATCCAGAATA-3′